

POLITECNICO DI TORINO

Master's Degree in Environmental and Land Engineering

Study of climate-related heat risks to public health in the Mediterranean region.

Supervisors Candidate

Prof. Jost-Diedrich GRAF VON HARDENBERG Alice AMERIO

Dott. Jacopo GRASSI

October 2025

Abstract

Climate change poses severe threats to human populations worldwide, with particularly strong impacts on health. Extreme events are becoming more frequent, intense, and prolonged as a consequence of global warming.

Among these, heat waves represent one of the most direct manifestations, with significant health implications.

This thesis focuses on the Mediterranean basin, identified as a 'climate change hotspot' due to its warming rates higher than other zones, and high population density.

An ensemble of nine climate models from the Coupled Model Intercomparison Project Phase 6 (CMIP6) was employed to assess future temperature trends under two Shared Socioeconomic Pathways (SSP2-4.5 and SSP5-8.5) and three time horizons (short: 2021-2040, medium: 2041-2060, long: 2081-2100), and compared with the historical baseline (1981-2010). Daily maximum near surface air temperature (tasmax) was chosen as indicator of heat waves. Future temperature distributions were combined with a Relative Risk (RR) function to estimate excess mortality, defined as the percentage increase relative to baseline mortality.

Hazard was determined from deviations above the Optimum Temperature (T_{opt}) , vulnerability with the RR function, while exposure was considered through population data, since climate risk assessment derives from interactions among these three factors.

Ensemble mean and uncertainty among models were determined, showing higher uncertainty values along coastlines. In addition, some cities were analyzed, selected for their different locations, climatic conditions and population.

The results confirm an increase in mortality due to heat, reaching values of 3% with respect to baseline mortality, under the SSP5-8.5 long-term scenario. Areas at higher risk were identified through a synthetic index, which allows the combination of future population exposure and future excess mortality.

This analysis adopts a method already used in the literature, though not previously applied to such extended regions, providing insights into the health implications of global warming in one of the world's most vulnerable regions and offering a framework that could be developed in future studies.

Table of Contents

1	Inti	roduct	ion	1
	1.1	Clima	te Risks	2
	1.2	Extre	me Heat Events	4
	1.3	Medit	erranean Region	5
2	Dat	a and	Methods	10
	2.1	CMIP	6 Climate Models	10
	2.2	Mater	ials	14
	2.3	Study	Area	16
	2.4	Metho	odology	18
		2.4.1	Optimum Temperature	18
		2.4.2	Probability Distribution of Future Temperatures	18
		2.4.3	Relative Risk function	19
		2.4.4	Excess mortality estimation	20
3	Res	\mathbf{ults}		22
	3.1	Histor	rical Optimum Temperature and Future Distributions	22
	3.2	Exces	s mortality and Population Exposure	31
4	Dis	cussio	ns and Conclusions	35
Re	efere	nces		38
\mathbf{A}	Apı	oendix	\mathbf{A}	43

List of Figures

1.1	Observed global mean surface temperature (GMST) from IPCC datasets, relative to the average temperature of 1850–1900 in each dataset.	
	Source: Figure 1.12 in [5]	1
1.2	Schematic representation of the components of climate risks, showing interactions between hazard, exposure and vulnerability. Source: Figure	
	SPM.1 in [7]	5
1.3	Climate and natural land ecosystems in the Mediterranean Basin, based on Köppen-Geiger climate types, for the baseline climate (a, 1985–2014)	
	and the future climate (b, 2076–2100). Source: Figure CCP4.4 in [14].	6
1.4	The Mediterranean region topography and bathymetry (colour bar in metres), main urban areas (population in thousands for 2020, container	
	ports (millions of TEU [twenty-foot container equivalent units] in 2017.	
	Source: Figure CCP4.1 in [14]	7
2.1	Schematic representation of a three-dimensional grid of cells, each one represented by mathematical equations governing material and energy	
	fluxes. Source: [20]	11
2.2	Scenario matrix showing combinations of socioeconomic development pathways and climate outcome expressed as radiative forcings. Source:	
	[23]	12
2.3	Map of the Mediterranean Basin study area, showing the focus cities	1.0
2.4	with red markers	16
2.4	Relative risk of excess mortality as a function of deviation from optimum	
	temperature. The vertical dashed line indicates T_{opt}	19
3.1	${\it Mean value of the historical } 84^{th} \ percentile \ of \ daily \ maximum \ temperature.$	22
3.2	Coefficient of Variation (CV) of the historical 84 th percentile of daily	
	maximum temperature	23
3.3	PDFs of daily maximum temperature for Cairo: on the left SSP2-4.5, on the right SSP5-8.5	24
2 1	CDFs of daily maximum temperature for Cairo: on the left SSP2-4.5,	2
3.4	on the right SSP5-8.5	24
9 5		۷4
3.5	PDFs of daily maximum temperature for Istanbul: on the left SSP2-4.5,	o.
	on the right $SSP5$ -8.5	25

LIST OF FIGURES

3.6	CDF's of daily maximum temperature for Istanbul: on the left SSP2-4.5,	
	on the right SSP5-8.5	25
3.7	PDFs of daily maximum temperature for Barcelona: on the left SSP2-	
	4.5, on the right SSP5-8.5	26
3.8	CDFs of daily maximum temperature for Barcelona: on the left SSP2-	
	4.5, on the right SSP5-8.5	26
3.9	PDFs of daily maximum temperature for Athens: on the left SSP2-4.5,	
	on the right SSP5-8.5	26
3.10	CDFs of daily maximum temperature for Athens: on the left SSP2-4.5,	
	on the right SSP5-8.5	27
3.11	PDF of daily maximum temperature for Turin: on the left SSP2-4.5,	
	on the right SSP5-8.5	27
3.12	CDF of daily maximum temperature for Turin: on the left SSP2-4.5,	
	on the right SSP5-8.5	28
3.13	PDF of daily maximum temperature for Madrid: on the left SSP2-4.5,	
	on the right SSP5-8.5	28
3.14	CDF of daily maximum temperature for Madrid: on the left SSP2-4.5,	
	on the right SSP5-8.5	28
3.15	PDF of daily maximum temperature for Belgrade: on the left SSP2-4.5,	
	on the right SSP5-8.5	29
3.16	CDF of daily maximum temperature for Belgrade: on the left SSP2-4.5,	
	on the right SSP5-8.5	29
3.17	PDF of daily maximum temperature for Rome: on the left SSP2-4.5,	
	on the right SSP5-8.5	29
3.18	CDF of daily maximum temperature for Rome: on the left SSP2-4.5,	
	on the right SSP5-8.5	30
3.19	Mean of excess mortality (%) for the two scenarios (SSP2-4.5 in the	
	first row, SSP5-8.5 in the second row) and the three time horizons:	
	short (first column), medium (second column) and long term (third	
	column)	31
3.20	CV of excess mortality (%) for the two scenarios (SSP2-4.5 in the first	
	row, SSP5-8.5 in the second row) and the three time horizons: short	
	(first column), medium (second column) and long term (third column)	
	with red marker indicating zones of higher uncertainties	32
3.21	Population of considered cities as a function of T_{opt} and mean excess	
	mortality (%) for the two scenarios (SSP2-4.5 in the first row, SSP5-	
	8.5 in the second row) and the three time horizons: short (first column),	
	medium (second column) and long term (third column). Marker size	
	proportional to city population	32
3.22	Z-score to combine excess mortality with population density for short-	
	term and two scenarios: SSP2-4.5 on the left and SSP5-8.5 on the	
	right	33

LIST OF FIGURES

3.23	Z-score to combine excess mortality with population density for medium-	
	term and two scenarios: SSP2-4.5 on the left and SSP5-8.5 on the	
	right	33
3.24	Z-score to combine excess mortality with population density for long-	
	term and two scenarios: SSP2-4.5 on the left and SSP5-8.5 on the	
	right	34
A.1	Population density (log10) related to excess mortality mean (%): SSP2-	
	4.5 in the first row, SSP5-8.5 in the second row and the three time	
	horizons: short (first column), medium (second column) and long term	
	$(third\ column)$	43

List of Tables

2.1	List of the nine Global Climate Models (GCMs) used in this study. $\ . \ .$	15
2.2	Population dataset characteristics	15

Chapter 1

Introduction

Climate change has been described as 'the biggest global health threat of the 21st Century', putting the lives and well being of billions of people worldwide at increased risk [1].

According to the Intergovernmental Panel on Climate Change (IPCC) Sixth Assessment Report (AR6), approximately 3.3 to 3.6 billion people live in contexts that are highly vulnerable to climate change [2].

Global temperature is the most commonly used metric to summarize the state of the climate [3], since it has increased substantially compared to preindustrial levels, as shown in Figure 1.1 [4].

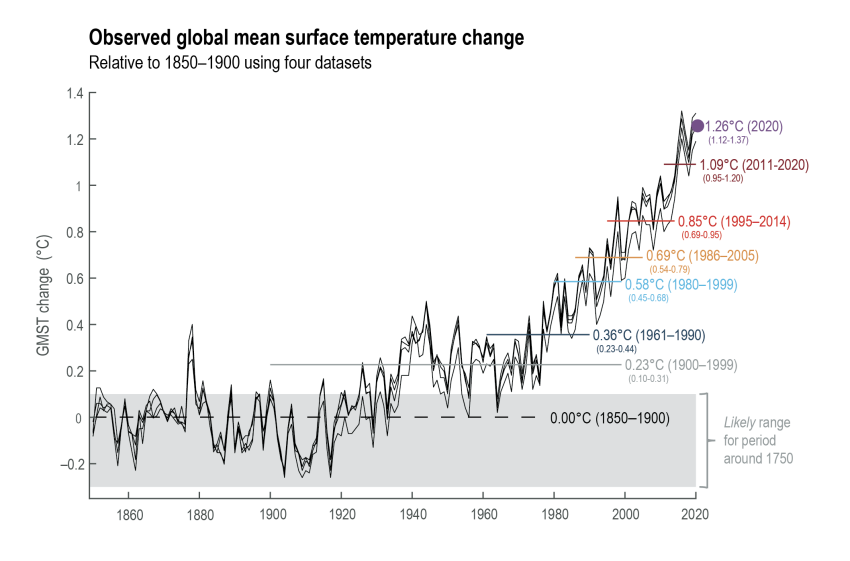


Figure 1.1: Observed global mean surface temperature (GMST) from IPCC datasets, relative to the average temperature of 1850–1900 in each dataset. Source: Figure 1.12 in [5].

Global warming has contributed to an increase in the frequency, intensity, and duration of extreme heat events, or heatwaves [1], which are typically measured by temperature extremes.

Exposure to heat has devastating effects on human health, contributing to increased morbidity (illness) and mortality in different geographical locations [1].

In this context, the Mediterranean Basin has been identified as one of the regions most affected by future climate change impacts [6].

Extreme climate events alone are not sufficient to assess the consequences of climate change, as the severity of impacts is strongly influenced by the exposure and vulnerability of affected systems [7].

Therefore, climate change impacts are most appropriately quantified through a risk assessment approach, which considers the interactions among extreme events, exposure, and vulnerability [7].

1.1 Climate Risks

Climate risks are defined as the potential for adverse consequences for human or ecological systems, including impacts on lives, health, well being, infrastructures, and services [8].

In the context of climate change, risks result from dynamic interactions between climate-related hazard, with the exposure of affected human or ecological systems, and their vulnerability [8].

This framework is illustrated in Figure 1.2, which determines the role of natural climate variability and anthropogenic changes, as well as the exposure and vulnerability of human society and natural ecosystems in determining climate risks [7].

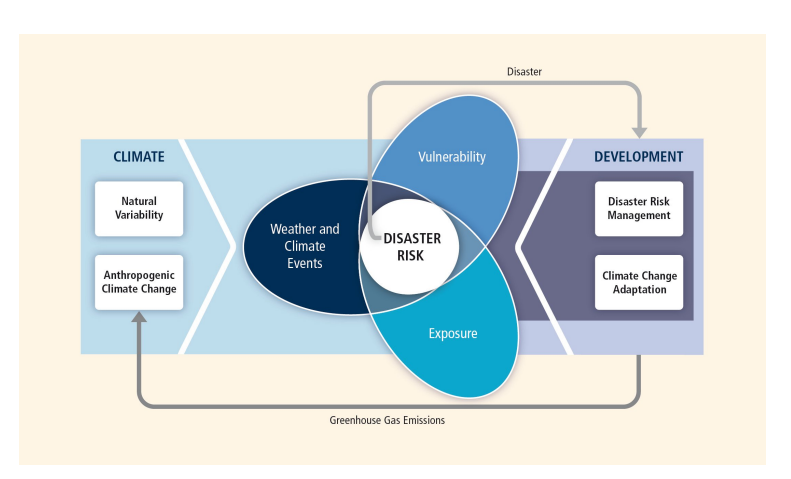


Figure 1.2: Schematic representation of the components of climate risks, showing interactions between hazard, exposure and vulnerability. Source: Figure SPM.1 in [7].

According to IPCC definitions, these three elements can be described as follows:

- Hazard refers to the potential occurrence of natural or human-induced physical events that may cause health impacts [8];
- Exposure indicates the presence of people, livelihoods, species or ecosystems that could be adversely affected [8];
- Vulnerability represents the propensity or predisposition of exposed elements to be adversely affected [8].

Currently, no universally accepted risk analysis method exists for all phenomena and uses; the choice of the method depends on their relevance, utility, and available resources [9].

Three main approaches are commonly used for risk assessment: deterministic, semi-quantitative, probabilistic [9].

Deterministic methods consider the impacts of defined risk events to determine whether consequences are manageable. They are particularly useful when a full stochastic approach is not feasible due to limited data. They are not completely reliable, as they consider only a subset of potential events, but their performance in preventing impacts from hazard is generally good and, in some cases, better than other methods [9]. They may be referred to as a scenario test, a stress test, or a reverse stress test [9].

- Scenario test, where a defined event or series of events is postulated and the consequences are assessed;
- Stress test, with pre-agreed assumptions of risk, for example implied within a business plan which are stressed and challenged to determine their impact on results;
- Reverse stress test, where events or combinations of events are postulated that could cause insolvency of the firm [9].

If properly presented, they can be clear, transparent, and understandable [9].

Semi-quantitative approaches categorise risks using comparative scores rather than explicit probability or measurable consequences. They are more rigorous than purely qualitative methods but do not constitute a full quantitative risk analysis. Semi-quantitative methods can illustrate comparative risk and consequences in an accessible way to users. A risk matrix is used to communicate a semi-quantitative assessment: a combination of two dimensions of risk, severity and likelihood, which allows a simple visual comparison of different risks. Severity is estimated from minor to catastrophic, and likelihood from rare to almost certain. These methods can be a useful stepping stone toward a full quantitative system, particularly where detailed data are lacking. They provide a framework to capture subjective opinions, challenge them, and identify areas requiring additional analytical effort [9].

Probabilistic risk analysis typically associates probability distributions to frequency and severity elements of hazards and then runs many simulated events or years to assess the likelihood of loss at different levels. These methods are widely adopted by the insurance industry, especially for complex or catastrophic natural hazard risks. The main advantage is that they consider frequency and severity together in a more comprehensive and complex way than other methods, while the main limitation is the difficulty in obtaining complex data on hazard, exposure, and vulnerability [9].

1.2 Extreme Heat Events

Extreme heat events are periods of abnormally high ambient temperatures [10], often referred to as heat waves, although the two terms are not strictly equivalent.

The IPCC defines heatwaves as periods of unusually hot weather, typically characterized with reference to a relative temperature threshold, and lasting from a few days to months [8]. This threshold is often determined using a percentile of daily maximum temperatures, or a fixed value [11].

In this thesis, the analysis focuses on extreme heat events, without considering a minimum number of consecutive hot days.

Extreme heat is among the most significant natural disasters globally, after floods, storms, and earthquakes in terms of impacts. In recent years, the frequent occurrence of extreme heat events has caused substantial adverse effects, particularly on human health [12].

Extreme heat events can be analyzed using the risk assessment framework, identifying and defining the three key determinants: hazard, exposure, and vulnerability.

Heat hazards include the frequency, intensity, and spatial extent of extreme heat events, as well as their potential socioeconomic, environmental, and health impacts, which are closely associated with rising ambient temperatures [12].

Temperature values are commonly used to quantify the risks for human populations due to extreme heat events [12].

The frequency and intensity of hot extremes have increased globally since 1950, while those of cold extremes have decreased [13]. The number of hot days and nights, as well as the duration, frequency, and intensity of extreme heat events is projected to increase over most land areas [13]. Although the magnitude of these trends varies depending on the region, spatial and temporal scales, and the metric considered, the evidence of a global warming effect is robust and consistent. In particular, increases in the intensity and frequency of hot extremes are almost always associated with higher temperatures and more extreme heat days [13].

The risk posed by extreme heat, as for other extreme climate events, is a function of the severity of the hazard and the exposure and vulnerability of the population [7]. Extreme heat events do not necessarily lead to extreme impacts, if exposure and vulnerability are low [7].

Heat exposure describes the frequency and intensity of human exposure to extreme heat, reflecting the degree to which individuals are in hazardous environments or potentially dangerous situations [12]. The key to assessing heat exposure is to identify and quantify this degree of exposure, using primary indicators, including the urban built environment and economic factors. Temperatures vary depending on land use or land cover type, with particularly elevated values in urban areas. Urbanization and the Urban Heat Island (UHI) effect have extended the duration of urban heat events, increasing the likelihood of residents being exposed to extreme heat [12]. Areas with high population density and low greenspace coverage exhibit the highest levels of exposure. Identifying these areas helps identify vulnerable regions and populations,

facilitating the development of targeted mitigation strategies [12].

Heat vulnerability refers to the degree of risk faced by specific regions or populations due to a lack of resources to effectively cope with or mitigate negative impacts of extreme heat [12]. Vulnerability results from both internal and external factors. Internal vulnerability includes population characteristics and health conditions, such as age, gender, and physiological state. This is particularly relevant for groups such as the elderly, children, pregnant women, and individuals with chronic diseases. This vulnerability is exacerbated in densely populated areas owing to the urban heat island effect and limited cooling resources. External vulnerability encompasses factors such as economic status, educational level, living conditions, and the distribution of critical infrastructure [12].

1.3 Mediterranean Region

The Mediterranean Basin is recognized as a 'climate change hotspot', due to the projected increase in climate hazards, in combination with high regional vulnerability and exposure [14].

The region lies in a transition zone between the arid climate of North Africa and the typical temperate and rainy climate of central Europe, and it is affected by interactions between mid-latitude and tropical processes [15].

Even relatively minor modifications of the general circulation - such as shifts in the location of mid-latitude storm tracks, or sub-tropical high pressure cells - can lead to substantial changes in the climate (Figure 1.3). Indeed, the Mediterranean region has shown large climate shifts in the past, and has been identified as a prominent hotspot in future climate change projections. The Mediterranean climate is characterized by mild and wet winters and hot dry summers [15].

Winter climate is mostly dominated by the westward movement of storms originating over the Atlantic, and impinging upon the Western European coasts, and in addition to this, also Mediterranean storms can be produced internally [15]. During summer, high pressure and descending motions dominate over the region, leading to dry conditions, particularly over the Southern part of the region; summer variability has been found to be connected with both the Asian and the African monsoons [15].

In addition to planetary scale processes and teleconnections, the climate of the Mediterranean is affected by local processes, induced by the complex physiography of the region, and the presence of a large body of water, the Mediterranean Sea [15].

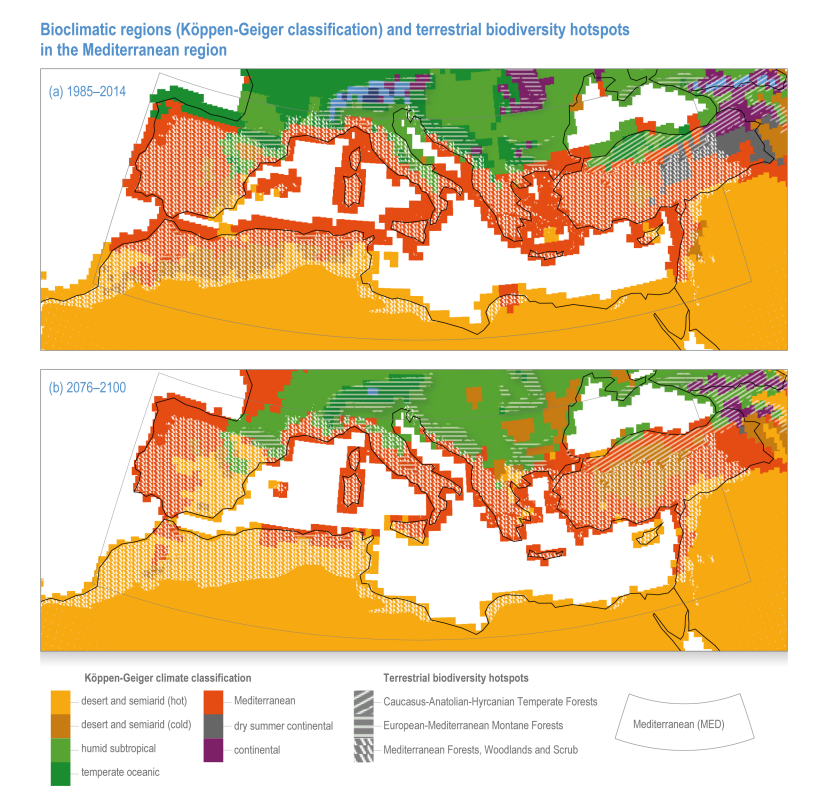


Figure 1.3: Climate and natural land ecosystems in the Mediterranean Basin, based on Köppen-Geiger climate types, for the baseline climate (a, 1985–2014) and the future climate (b, 2076–2100). Source: Figure CCP4.4 in [14].

The Mediterranean Sea is the largest of the semi-enclosed European seas, covering 2.6 million km², corresponding to 0.82% of the world's ocean surface [16].

Surrounded by 22 different countries, along 46000 km of coastlines, the region hosts around 500 million people living across three continents, Africa, Asia and Europe [16].

The countries in the Mediterranean Basin hosted approximately 542 million people in 2020, and this number is projected to increase to 657 million by 2050, and 694 million by 2100, according to the IPCC projections [14].

Moreover, in 1950, only 23.7% of the population lived in countries of the south, and this number increased to 41.2% in 2000, 43.6% in 2020, and is projected to reach 55.5% in 2050 and 64.6% in 2100 [14].

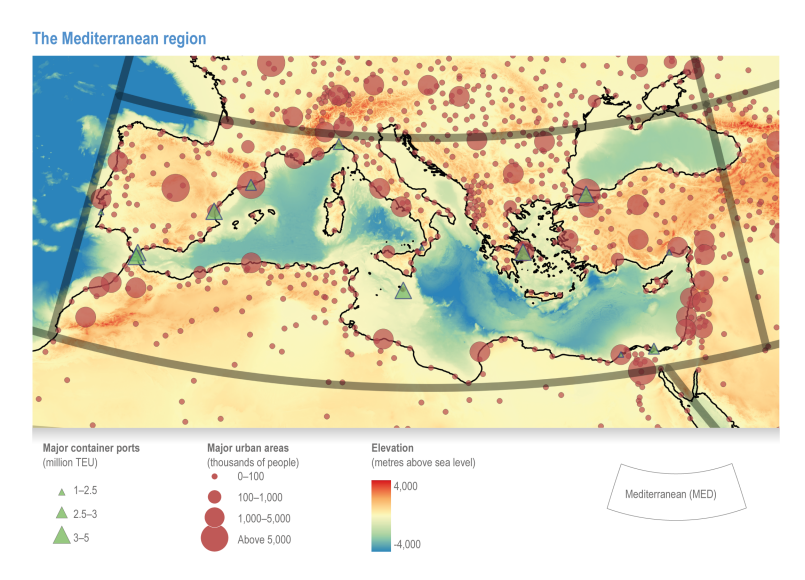


Figure 1.4: The Mediterranean region topography and bathymetry (colour bar in metres), main urban areas (population in thousands for 2020, container ports (millions of TEU [twenty-foot container equivalent units] in 2017. Source: Figure CCP4.1 in [14].

The annual mean temperatures of the basin are now 1.4°C above preindustrial levels and higher than the global mean warming [17]. So, the region is undergoing a warming trend, with longer and warmer summers and with consequent increase in the frequency and severity of heat waves [17].

With significant gaps in the socio-economic levels among the Mediterranean countries, particularly between the North and South, and in parallel with population growth and migration, the region is also facing increasing water demand under conditions of decrease in water availability and quality, ecosystems degradation and increased risk for forest fires [17].

These factors contribute to increasing vulnerability of the Mediterranean population to health risks. Since health impacts largely arise due to exposure and vulnerability, they are enhanced by climate change. These additional climate-related stressors create increased risks and make the communities of the Mediterranean Basin more vulnerable [17].

In the Mediterranean Basin, the three determinants of risks - hazard, exposure, vulnerability - interact explaining why the region is considered among the most affected by climate change [18].

Heat waves and temperature extremes are projected to intensify, with the regional average warming exceeding the global mean value by 20%. This trend causes changes in all other climate system components: in last decades, dry conditions have also become more frequent, with a large reduction of glaciers across high mountains of the Mediterranean [18]. Total annual precipitation is expected to decrease over most of the region, with dry conditions further enhanced by increasing evapotranspiration over land [18]. At the same time, increasing extreme events will become more frequent over large part of the Mediterranean [18].

Mediterranean mean sea level is projected to be, at the end of the 21^{st} century, in

the range from 20 to 110 cm higher than at the end of the 20^{th} century, depending on the level of anthropogenic emissions [18]. Widespread seawater warming and acidification will continue, with marine heat waves becoming longer, more intense and with increasing spatial extent [18].

Climate models also project that the Hadley Cell circulation will change, with the tropics expanding, and the mid-latitude westerlies and associated storm tracks will likely shift poleward [18]. Hadley circulation is a direct, thermally driven overturning cell in the atmosphere, consisting of poleward flow in the upper troposphere, subsiding air into the subtropical anticyclones, return flow as part of the trade winds near the surface, and with rising air near the equator in the so-called Inter-tropical Convergence Zone [8].

This is expected to enhance subsidence and reduce storminess at the latitudes of the Mediterranean region, with a resulting reduction in precipitation [18].

Projected changes in extreme temperature indicators suggest that the frequency and severity of heat extremes will increase. According to projections, summer daily maximum temperature is expected to increase up to 7°C by the end of the 21^{st} century in comparison with the recent past. Besides warmer daytime temperature maxima, parts of the Mediterranean will likely face an increase of more than 60% in the number of tropical nights. Increase of warm temperature extremes will be dramatic particularly in summer and with a 4°C global warming almost all nights will be warm and there will be no cold days. Warming is projected to be milder in winters and much stronger during summers. This is mainly attributed to land-atmosphere interactions and the transition to drier conditions [18].

As previously indicated, about 500 million people live in this area, and this trend is projected to increase in next decades, with differences in population distribution [14]. One-third of the Mediterranean population (about 150 million people) currently lives close to the sea, often in growing urban regions and with infrastructure vulnerable to sea level rise. Future exposure to sea level rise is related to demographic growth. All future projections indicates an increase of coastal population in the Mediterranean region to 2050. By 2100, coastal population could grow by up to 130%, mostly in the south. Overall, countries in the southeastern Mediterranean are most vulnerable to coastal risks, but the exposure is also high in the northern Mediterranean [14]. The coastal population growth projected until 2050 mostly occurs in southern Mediterranean countries, with Egypt, Libya, Morocco and Tunisia being the most exposed countries to future sea level rise [14].

Mediterranean cities are growing due to increasing population and socio-economic change, notably on the coasts of southern countries [18]. Impacts of climate change on urban areas are expected to be disproportionally high due to a concentration of population and assets – especially in high-risk prone areas - in combination with hazard-amplifying conditions [18].

The vulnerability of population to the impacts of environmental and climate change is strongly influenced by population density, level of economic development, food availability, income level and distribution, local environmental conditions, pre-

existing health status, and the quality and availability of public health care [18]. Vulnerable Mediterranean populations include the elderly, the poor, and people with pre-existing or chronic medical conditions, displaced people, pregnant women and babies. People who are disadvantaged due to a lack of shelter, clean water, energy or food are more at risk from extreme events [18].

Heat waves are responsible for high mortality rates causing tens of thousands of premature deaths, especially in large cities and among the elderly. Heat-related morbidity and mortality has been partially reduced in recent years by more efficient protection of people [18].

Most Mediterranean cities are compact and densely populated and have experienced strong impacts from extremely high temperatures on their population [18]. In recent decades, mortality rates due to heat stress have been reduced through national plans and alert systems that have raised risk awareness and avoidance among the population [18].

Urban areas along the Mediterranean coast are especially affected by climate change impacts on health, because these areas concentrate people and assets [18]. Urban areas often intensify climate-related hazards, in this case, hotter temperatures during extreme heat events, due to the urban heat island effect [18].

The European population at risk for heat stress is expected to increase (4% annually) in the coming years and could increase to 20 or to 48% by 2050, depending on different combinations of socio-economic scenarios. Vulnerability varies between regions, and the Mediterranean region will be among the most affected [18].

Chapter 2

Data and Methods

This chapter presents the data sources and the methodological framework adopted to assess projected health risks for the population in the Mediterranean Basin related to extreme heat events. According to the IPCC definition, climate risk results from the interactions of three components: hazard, vulnerability, and exposure.

Consequently, in this study, the risk to the population is expressed in terms of excess mortality, derived from the combination of these factors. Hazard is characterized by future temperature distributions, vulnerability is represented by a Relative Risk function to obtain excess mortality, and exposure information is added using population data.

2.1 CMIP6 Climate Models

Climate models are complex computer codes designed to simulate past, present, and future climate variability. They can be broadly defined as digital reproductions of the Earth system, aimed at reproducing the processes and interactions among its components [19].

The modelling framework represents climate variables on a three-dimensional grid of cells in the Earth's atmosphere, surface, and oceans (Figure 2.1). The three dimensions correspond to two horizontal directions (latitude and longitude), and one vertical direction. Each cell is characterized by specific horizontal and vertical resolutions, which determine the level of spatial detail provided by the model [20].

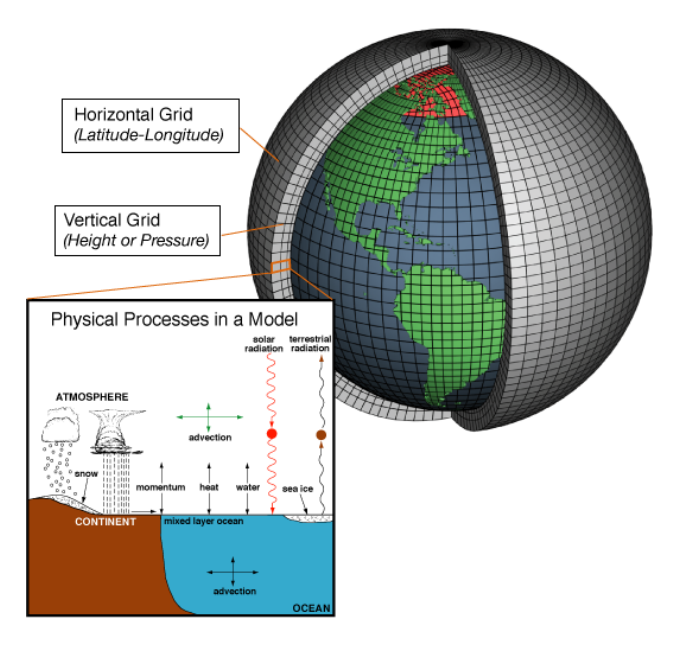


Figure 2.1: Schematic representation of a three-dimensional grid of cells, each one represented by mathematical equations governing material and energy fluxes. Source: [20].

Also known as General Circulation Models (GCMs), climate models use mathematical equations derived from fundamental laws of physics, fluid motion, and chemistry, to characterize how energy and matter interact in space and time. These equations are solved for each point of the grid, and the outputs are passed to neighboring cells, resulting in a representation of the exchange of mass and energy over time. In addition to spatial resolution, models are also characterized by temporal resolution, which depends on the size of the time steps: the smaller the time step, the more detailed the results [20].

While GCMs focus primarily on physical processes within the climate system, including atmospheric circulation models coupled with ocean circulation models [20], Earth System Models (ESMs) have been developed to extend this framework by incorporating biogeochemical processes and human actions that interact with the climate system [21].

ESMs additionally include representation of land surfaces, sea ice, aerosols, cloud physics, precipitation, evaporation and other water fluxes. This represents a major step forward in simulating the Earth's system [21].

Climate models provide a fundamental source of data for projecting possible future climate conditions [20].

The models used in this study belong to the Coupled Model Intercomparison Project Phase 6 (CMIP6), an international initiative that coordinates multi-model simulations from more than 50 modelling centers around the world. Outputs are publicly available through the Earth System Grid Federation (ESGF), enabling model comparison at a global level and improving knowledge about the climate system [22].

Among the different Model Intercomparison Project (MIP) experiments, historical simulations and future projections are considered in this analysis [22]. The former,

covering the period 1850-2014, are based on reconstructions of external forcings derived on observations. Future projections, instead, rely on forcings provided by the Integrated Assessment Models (IAMs), which harmonize them to ensure consistency with the historical baseline and across different forcings [22].

The sixth phase of CMIP introduces alternative scenarios, describing possible evolutions of anthropogenic drivers of climate change and consistent with socio-economic development. These are the Shared Socioeconomic Pathways (SSPs), which describe trajectories of future society development under the assumptions of no additional climate policy [23].

Unlike the Representative Concentration Pathways (RCPs), which formed the basis for climate projections in CMIP Phase 5 and consisted of four pathways describing land use and emission of greenhouse gases and air pollutants up to 2100, the SSPs represent a new set of scenarios for emissions and land use, produced using Integrated Assessment Models (IAMs) and based on pathways of societal development [23].

They are denoted as $SSPs_{x,y}$, where x identifies the specific socioeconomic pathway, and y indicates the global average radiative forcing level reached beyond 2100. Radiative forcings can be defined as changes in the net radiative flux, caused by changes in drivers of climate, such as changes in CO_2 concentrations or in the output of the Sun [8].

Among the available scenarios (Figure 2.2), two were selected for this analysis:

- SSP2-4.5, representing an intermediate pathway, with a stabilization of the radiative forcing at $4.5~\rm W~m^{-2}$ by the end of the century;
- SSP5-8.5, which is the highest emission pathway, producing a radiative forcing of 8.5 W $\rm m^{-2}$ by 2100 [23].

As the first number in each SSP indicates the general socioeconomic pathway (ranging from 1 to 5), the selected scenarios are based on the following assumptions: SSP2 represents the central pathway, in which trends continue their historical patterns without substantial deviations, without extreme land use and aerosol pathways; SSP5 assumes an energy intensive, fossil based economy and is the only scenario with emissions high enough to produce a radiative forcing of 8.5 W m⁻² by 2100 [23].

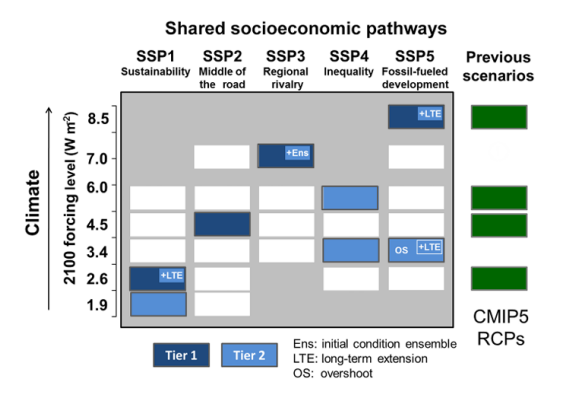


Figure 2.2: Scenario matrix showing combinations of socioeconomic development pathways and climate outcome expressed as radiative forcings. Source: [23].

Following the IPCC Assessment Report 6 (AR6) definition, these future scenarios were divided into three time horizons: [5]

• Short-term: 2021-2040;

 $\bullet \quad \text{Medium-term: } 2041\text{--}2060;$

• Long-term: 2081-2100.

2.2 Materials

For this study, among the available datasets, NEX-GDDP-CMIP6 was selected [24]. This dataset provides a set of global, high-resolution and bias corrected climate change projections derived from CMIP6, suitable for evaluating climate change impacts at local scales.

Downscaling of GCM outputs is required due to two main limitations of global simulation results. First, GCMs employ relatively coarse resolution grid (few degrees), which limits their ability to capture spatial details; second, they can exhibit local biases in spatial characteristics [24].

To address these limitations, the dataset is adjusted using Bias-Correction Spatial Disaggregation (BCSD) statistical method for downscaling [25]. This algorithm compares the original GCM outputs with corresponding climate observations over a common reference period and uses resulting information to adjust future climate projections. It uses spatial detail provided by observational datasets to interpolate the GCM outputs to higher-resolution grids. Development of the NEX-GDDP-CMIP6 utilized 0.25-degree daily-averaged data for each variable [24].

The dataset is distributed by the NASA Center for Climate Simulations (NCCS) and is publicly accessible at their official site [26]. Since the data are already biascorrected, no additional adjustments were applied in this analysis. The dataset provides climate projections for the period 2015-2100, covering four SSP scenarios: SSP1-2.6, SSP2-4.5, SSP3-7.0, and SSP5-8.5, with historical observations for the period 1950-2014. In this study, the historical baseline period 1981-2010 was adopted as reference.

Among the 35 GCMs available in this dataset, nine were selected, as shown in Table 2.1, to ensure representation of different modelling centers.

Maximum daily near-surface air temperature (tasmax) was selected among the nine available climate variables, as required by the methodological framework adopted in this study [27].

Table 2.1: List of the nine Global Climate Models (GCMs) used in this study.

Model	Modelling Centre	Resolution
		$(\mathit{lon}{ imes}\mathit{lat})$
ACCESS-CM2	Commonwealth Scientific and Industrial	$1.875^{\circ} \times 1.25^{\circ}$
	Research Organisation (CSIRO), Australia	
BCC-CSM2-MR	Beijing Climate Centre (BCC), China	$1.125^{\circ} \times 1.125^{\circ}$
CanESM5	Canadian Centre for Climate Modelling	$2.8^{\circ} \times 2.8^{\circ}$
	and Analysis (CCCma), Canada	
CMCC-CM2-SR5	Fondazione Centro Euro-Mediterraneo sui	1.25°×1.0°
	Cambiamenti Climatici (CMCC), Italy	
EC-Earth3	EC-Earth Consortium, Europe	1.0°×1.0°
FGOALS-g3	Chinese Academy of Sciences (CAS),	$2.0^{\circ} \times 2.25^{\circ}$
	China	
IPSL-CM6A-LR	Institut Pierre-Simon Laplace (IPSL),	$2.5^{\circ} \times 1.25^{\circ}$
	France	
MIROC6	Model for Interdisciplinary Research on	1.4°×1.4°
	Climate (MIROC), Japan	
MPI-ESM1-2-HR	Max Planck Institute for Meteorology	0.94°×0.94°
	(MPI), Germany	

While climate data characterize the hazard, risk assessment also requires information about exposure. Among the available global population datasets, gridded projections from the World Bank Climate Change Knowledge Portal (CCKP) were selected for this study (available at their official website [28]).

This dataset is consistent with the SSP scenarios used for climate projections, and has the same spatial resolution as NEX-GDDP ($0.25^{\circ} \times 0.25^{\circ}$).

Although climate projections follow the standard IPCC time horizons (2021-2040, 2041,2060, 2081-2100), the CCKP population data are provided for slightly shifted periods (2020-2039, 2040-2059, 2080-2099).

The main characteristics of the population dataset are summarized in Table 2.2.

Table 2.2: Population dataset characteristics.

Variable	Description
Population Count	Number of inhabitants per grid cell
Population Density	Inhabitants per km ²

2.3 Study Area

The geographical domain of the analysis is the Mediterranean Basin, bounded by 30°N-47°N and 10°W-40°E, shown in Figure 2.3.

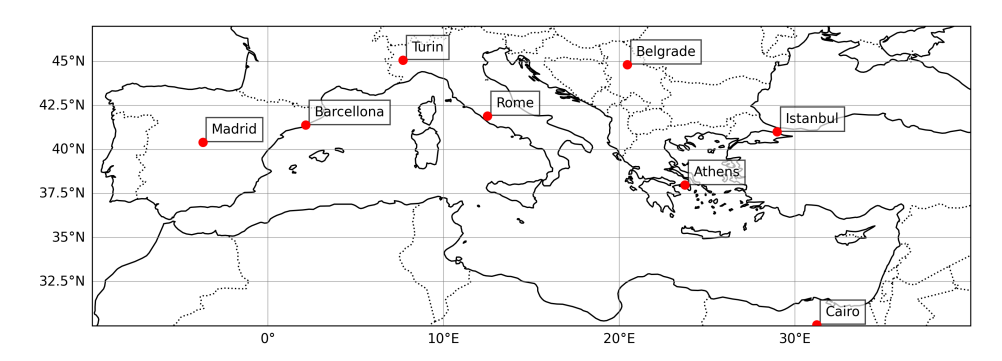


Figure 2.3: Map of the Mediterranean Basin study area, showing the focus cities with red markers.

Within this domain, the study focuses on different cities, selected to capture different climatic, geographic, and urban conditions across the region. The focus cities are:

- Turin, located in north-west part of Italy, is the fourth largest Italian urban area. Alpine mountains favour a limited circulation of foehn winds, conferring to the city a complex mosaic of microclimates [29].
- Rome is located along the western coast of the Italian peninsula. Characterized by temperate climate, with hot and dry summers, the atmospheric circulation is governed by the sea-breeze from the southwest [30].
- Madrid is located in the center of Spain, with altitudes ranging from 846 m in the north to 543 m in the southeast. These values, with the distance from the sea, cause a climate with scarce precipitation, and hot, dry summers [31].
- Barcelona is located along the coastline, and is one of the most densely populated urban area of the Mediterranean region with a population of 1.6 million inhabitants [32].
- Istanbul is characterized by Mediterranean climate, with hot summers, and not too cold winters. It is a densely populated metropolis, characterized by high concentration of buildings, with limited green spaces [33].
- Cairo is a densely populated megacity, characterized by increasing frequency and duration of heat waves, despite the common occurrence of high daily maximum temperatures [34].
- Athens' climate is mild, with dry and hot summers; it is a coastal city located in the Mediterranean [35].

• Belgrade is characterized by continental climate, influenced minimally by the sea, and showing increasing trend in temperature values [36].

Coastal cities were selected for their population growth: Rome, Athens and Barcelona increased less than twofold between 1950-2010, and in the same period, Istanbul grew 15-fold, while Cairo approximately 4-fold [16].

Heat waves are responsible for high mortality rates causing tens of thousands of premature deaths, especially in large cities and among the elderly. Most Mediterranean cities are compact and densely populated, and have experienced strong impacts from extremely high temperatures on their population [18].

2.4 Methodology

This section describes the methodology adopted in this study to assess future excess mortality, quantifying the risks to Mediterranean population associated with extreme heat events.

The approach integrates the three components of climate risk. First, the hazard is quantified by projecting future temperature distributions, relative to historical data (Optimum Temperature, T_{opt}). Second, population vulnerability is assessed using a Relative Risk function, linking increasing temperatures with health impacts.

2.4.1 Optimum Temperature

As previously described, the first step of the analysis involves the evaluation of the climate hazard, here represented by future distributions of daily maximum temperature tasmax. A central element of this step is the definition of the Optimum Temperature (T_{opt}) , which represents the threshold above which heat begins to pose significant risk to human health.

Following epidemiological studies for temperate climates [37], T_{opt} was defined as the 84^{th} percentile of the historical distribution of the daily maximum temperature (1981-2010). The choice of this value was based on the study followed for this analysis [27], which found that the optimum temperature can be estimated using the $80-85^{th}$ percentile of daily maximum temperatures. The T_{opt} estimated (based on cities in Japan), corresponded to the mean value, and in most cases, it was around the 84^{th} percentile [27]. To repeat the study applying it to the Mediterranean region, the same value for T_{opt} was selected. This value is aligned with another study [37], which found slightly different values, depending on the considered country (79th percentile for Italy, 78^{th} percentile for Spain). In fact, the definition of T_{opt} as the 84^{th} percentile provides a standardized approach, but it may not capture differences at local level [37]. Optimum temperature value differs regionally among cities and regions, according to their climate [38].

2.4.2 Probability Distribution of Future Temperatures

To quantify the heat hazard, the distribution of projected daily maximum temperatures was evaluated relative to T_{opt} .

For each grid cell, Probability Density Functions (PDFs) of daily maximum temperature were constructed by dividing the observed temperature range into 100 equally spaced bins and computing normalized histograms [27].

This approach provides an intuitive representation of the hazard: by comparing historical and future PDFs, one can directly visualize both the increasing probability of exceeding T_{opt} and the shifting occurrence of extreme temperatures.

The analysis was performed using a multi-model approach, by computing the mean of temperatures (T_{opt}) across the selected models and quantifying spatial variability using the Coefficient of Variation (CV).

The CV, also known as relative standard deviation, is a dimensionless statistical metric that expresses the degree of dispersion of values relative to the mean. Mathematically, it is defined as the ratio between the standard deviation (σ) and the mean (μ) and is commonly reported as a percentage.

$$CV = \frac{\sigma}{\mu} \times 100$$

Where the standard deviation (σ) quantifies the spread of data around the average, while the mean (μ) represents the central tendency of the data set [39].

2.4.3 Relative Risk function

The health implications of exceeding T_{opt} were quantified using a Relative Risk (RR) function, linking mortality to the deviation from the optimum temperature $\Delta T = T - T_{opt}$.

The RR function was initially defined as a stepwise relationship from epidemiological studies and then smoothed using a Piecewise Cubic Hermite Interpolating Polynomial (PCHIP). This ensures monotonicity and prevents unrealistic oscillations, producing a curve that is statistically sound and epidemiologically plausible [27].

Only positive deviations from T_{opt} were considered, as cold-related mortality was outside the scope of this study.

Figure 2.4 shows a Relative Risk function, highlighting how even moderate deviations above T_{opt} can lead to a sharp increase in mortality risk.

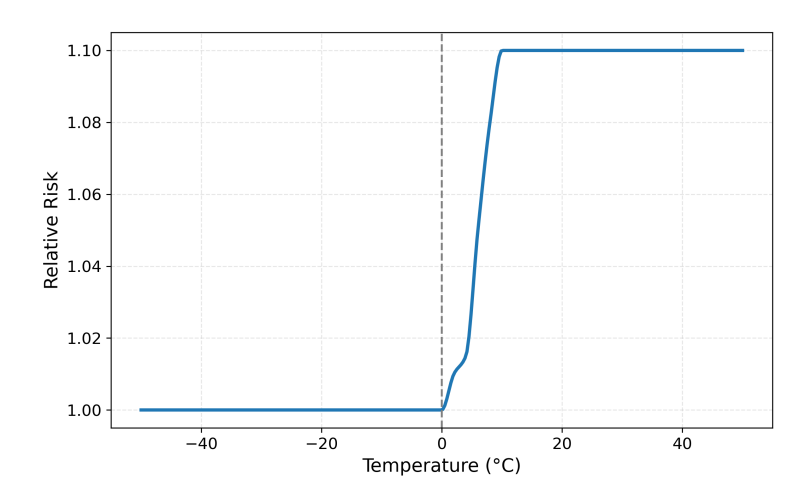


Figure 2.4: Relative risk of excess mortality as a function of deviation from optimum temperature. The vertical dashed line indicates T_{opt} .

The graph shows the relation between positive deviations from the optimum temperature (x-axis), and the Relative Risk (y-axis). The risk remains close to 1.00 for temperature below T_{opt} , rapidly increasing above this threshold. The risk rapidly increases for small deviations from optimum temperature, reaching a maximum value of 1.10 for an increase of 10°C from T_{opt} value. Then, the curve remains stable at 1.10 for increasing temperature values, reflecting saturation of relative risk for extreme

temperatures. In this study, the delay effect is not considered, and the function reflects the maximum instantaneous increase, rather than distributed effects [27].

It is important to consider that the RR function is based on limited epidemiological studies, and its extrapolation to the Mediterranean region may introduce uncertainty, representing a weakness for the followed method [27].

2.4.4 Excess mortality estimation

Excess mortality was estimated for each grid cell by combining the probability density function of temperature exceeding the optimum value, T_{opt} , with the corresponding relative risk function.

For each grid cell, excess mortality is defined as:

$$M(\text{lat}, \text{lon}) = \sum_{\text{bins}} PDF(T) \cdot RR(T - T_{opt} - 1) \cdot \Delta T.$$

It was estimated for each grid cell by combining the probability density function of temperatures with the corresponding relative risk function, weighting each bin by its width, ΔT .

The calculation was repeated across the nine selected models, two emission scenarios, and three time horizons. Ensemble mean and Coefficient of Variation were computed to capture both central estimates and associated uncertainty.

To account for exposure, excess mortality grids were combined with population density maps. This integration highlights areas where heat effects are amplified by high number of inhabitants, identifying regions at higher risk.

To provide a metric to capture both projected excess mortality and population exposure, a synthetic index was developed. For each grid cell, two variables were considered: mean excess mortality (%) and population density (\log_{10}). Each variable was standardized using Z-scores, using the following formula:

$$Z = \frac{X - \mu}{\sigma}$$

where X is the observed measurement, μ is the mean of all measurements, and σ is the standard deviation. Standardization ensures comparability between variables with different units. Z-scores were computed separately for excess mortality and population density, and then aggregated. The final index is obtained by summing the two variables attributing equal weight.

Cells with positive Z-score values represent regions where both excess mortality and population density are above the mean, while negative values indicate areas with lower combined risk [40].

This approach differs from the Heat Vulnerability Index (HVI), widely used in the literature, which typically considers demographic and socioeconomic factors, such as age distribution, poverty, health conditions, or access to green areas [41].

In contrast, the proposed index represents a simplification, focusing on the direct interaction between hazard and exposure, expressed as population density. This simplified formulation neglects important vulnerability factors, which are important to define how different people could adapt to increasing temperatures [41].

The proposed risk index is simple and directly linked to the number of people exposed: vulnerability has previously been considered with the Relative Risk function, and resulting index shows the relation between excess mortality and number of inhabitants per km².

By excluding socioeconomic and demographic factors, the index may underestimate the risk in different areas, neglecting percentage of elderly population, or urban areas with limited adaptive capacity.

In addition, the assumption of equal weight for mean excess mortality and population density is a simplification, whereas the contribution of these two factors may contribute in different ways to the final risk.

The methodology applied in this thesis can be classified as a semi-quantitative risk assessment approach, with excess mortality quantified under different climate scenarios and time horizons, combining hazard, exposure, and vulnerability according to the IPCC framework.

Chapter 3

Results

This chapter presents the main results of the analysis, with a particular focus on the relationships between historical optimum temperature (T_{opt}) , projected future temperature distributions, and associated risks for the Mediterranean Basin. The results are organized in two sections. The first examines the combination of hazard and vulnerability, while the second provides a risk assessment, considering also population exposure.

3.1 Historical Optimum Temperature and Future Distributions

As described in the previous chapter, the 84^{th} percentile of historical (1981-2010) daily maximum temperature (T_{opt}) was adopted as a reference value, representing the threshold above which the risk related to heat begins to increase [27].

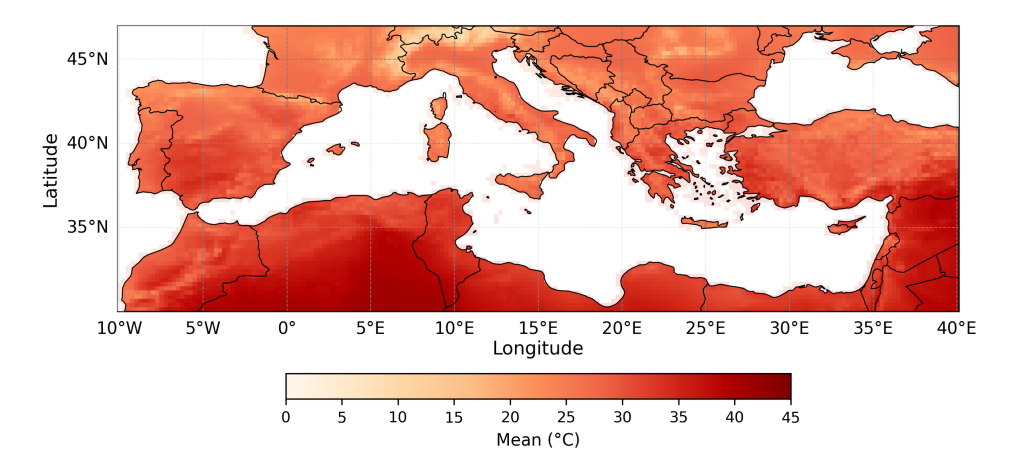


Figure 3.1: Mean value of the historical 84th percentile of daily maximum temperature.

Figure 3.1 shows that mean historical T_{opt} exhibits clear spatial heterogeneity across the Mediterranean Basin. Values reach up to 40° C in North Africa and the eastern part of the domain, while most continental European regions remain below 30°C. These differences reflect regional climatic conditions and population

acclimatization. In addition to climate, topography, demography, urban structure influence T_{opt} values [38].

Populations are to some extent acclimatised and, as far as their socio-economic conditions allows, behaviourally and technically adapted to their local climate, even to extremes [38]. The level of acclimatisation to temperature is significantly determined by regular exposure to a certain temperature [38].

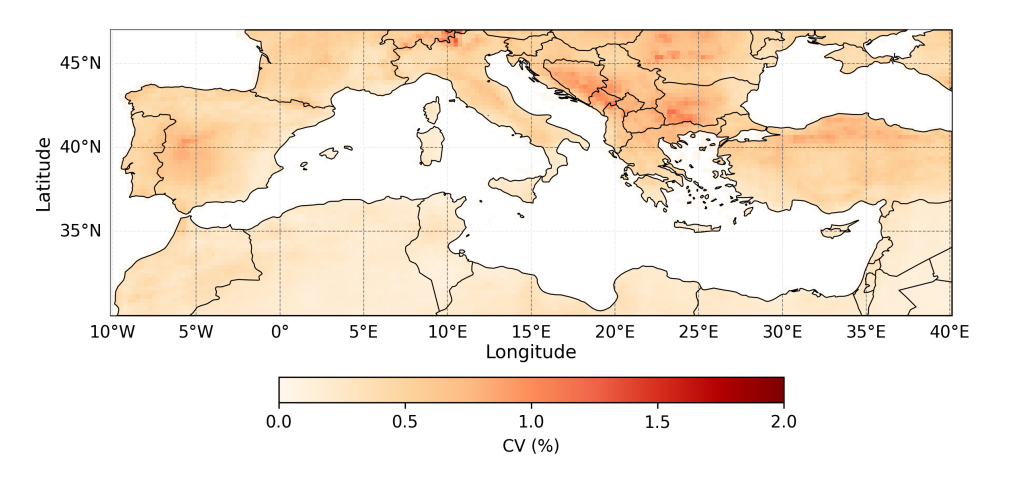


Figure 3.2: Coefficient of Variation (CV) of the historical 84th percentile of daily maximum temperature.

The CV (Figure 3.2) indicates relatively low variability among models in coastal areas. In contrast, inland regions - including the Iberian Peninsula, the Alps and the Balkans - show higher CV values, reaching 2% and highlighting increased inter-model variability.

These patterns provide a measure of confidence in the multi-model mean, helping to identify regions where projections are more or less robust [42]. Overall, the majority of the domain exhibits high model agreement, with higher variability confined to specific inland hotspots.

To better understand future hazard at urban scale, the Probability Density Functions (PDFs) and the corresponding Cumulative Distribution Functions (CDFs) of projected daily maximum temperatures were computed for the cities selected in Section 2.3.

While PDFs describe the probability of occurrence of specific temperature values, CDFs provide the probability of exceeding a given temperature threshold, in this case T_{opt} .

For each city, the PDF is presented alongside its corresponding CDF. Within each panel, SSP2-4.5 is shown on the left, and SSP5-8.5 on the right side, including their respective time horizons (short, medium, long term), together with the historical temperature distribution and T_{opt} , indicated by a dashed line.

The Southern Mediterranean and middle east, including cities of Cairo and Istanbul, exhibit the strongest warming trend, particularly under SSP5-8.5 for the long-term horizon.

The PDFs for Cairo (Figure 3.3) show marked shift toward higher temperatures,

with the CDFs (Figure 3.4) showing significant increase in the probability of exceeding T_{opt} , which passes from 15% of historical period, to 40% for the worst case. This trend reflects the rapid warming of the region, with increasing magnitude, duration and frequency of heat waves [43].

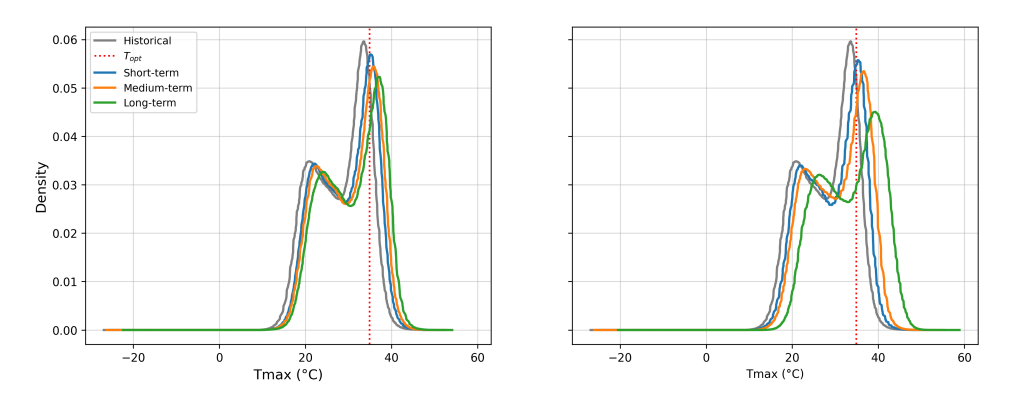


Figure 3.3: PDFs of daily maximum temperature for Cairo: on the left SSP2-4.5, on the right SSP5-8.5.

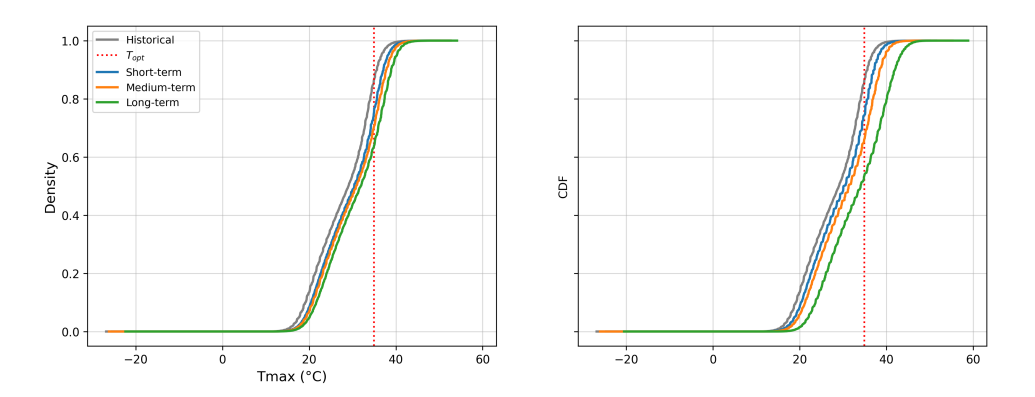


Figure 3.4: CDFs of daily maximum temperature for Cairo: on the left SSP2-4.5, on the right SSP5-8.5.

Istanbul shows similar patterns, even if the PDFs (Figure 3.5) show different temperature distributions compared to Cairo, reflecting cooler climatic conditions. The probability of exceeding T_{opt} is slightly lower (Figure 3.6), and corresponds to about 37% for the same worst scenario.

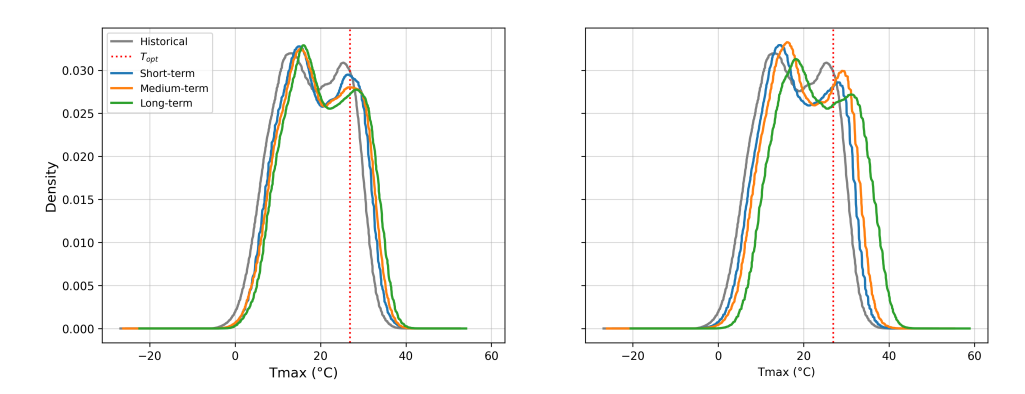


Figure 3.5: PDFs of daily maximum temperature for Istanbul: on the left SSP2-4.5, on the right SSP5-8.5.

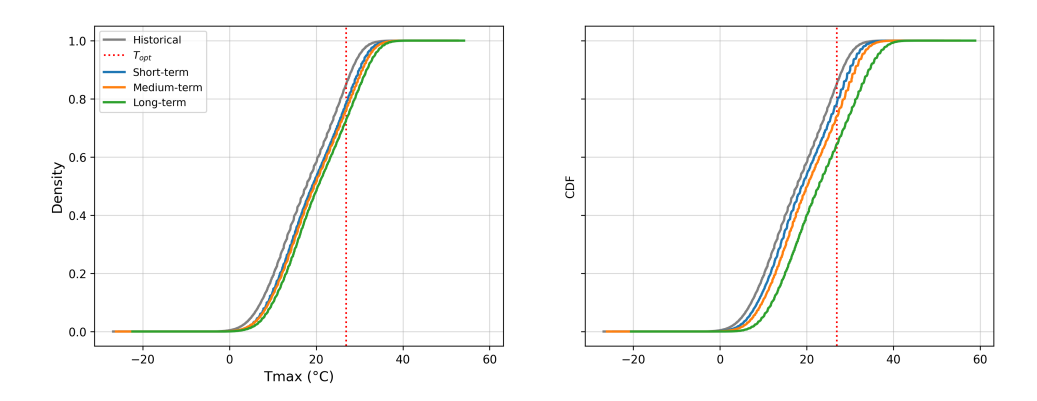


Figure 3.6: CDFs of daily maximum temperature for Istanbul: on the left SSP2-4.5, on the right SSP5-8.5.

Considering Mediterranean cities influenced by the sea, Barcelona and Athens show moderate warming trends compared to previously discussed cities.

Both cities are characterized by a typical Mediterranean climate - Barcelona in the western Mediterranean basin [32], and Athens in the eastern part [35] - and both are highly urbanized, which enhances the Urban Heat Island (UHI) effect. Projected trends indicate an increase in extreme temperature events, with the number of heatwaves days expected to rise from two days during 1961–1990 to approximately 40 days for 2071–2100 in Barcelona [32]. The PDFs of Barcelona and Athens show similar temperature distributions, with Athens showing higher PDF values in the 30°C-40°C range, highlighting generally hotter climatic conditions.

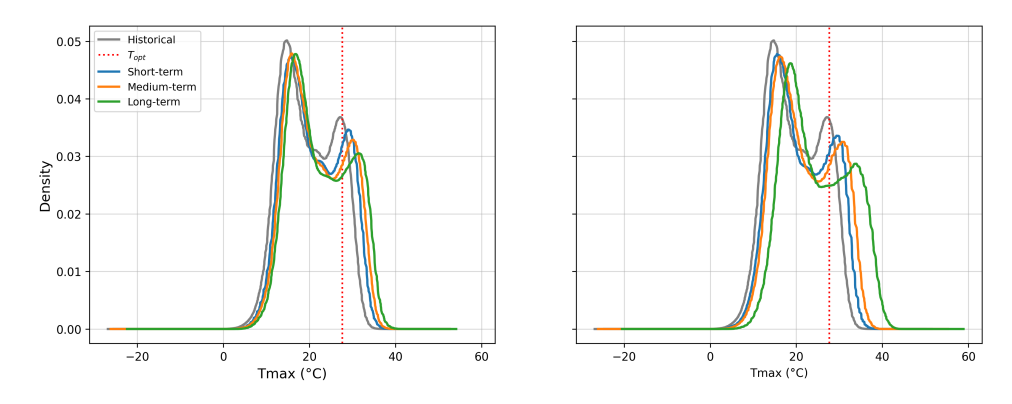


Figure 3.7: PDFs of daily maximum temperature for Barcelona: on the left SSP2-4.5, on the right SSP5-8.5.

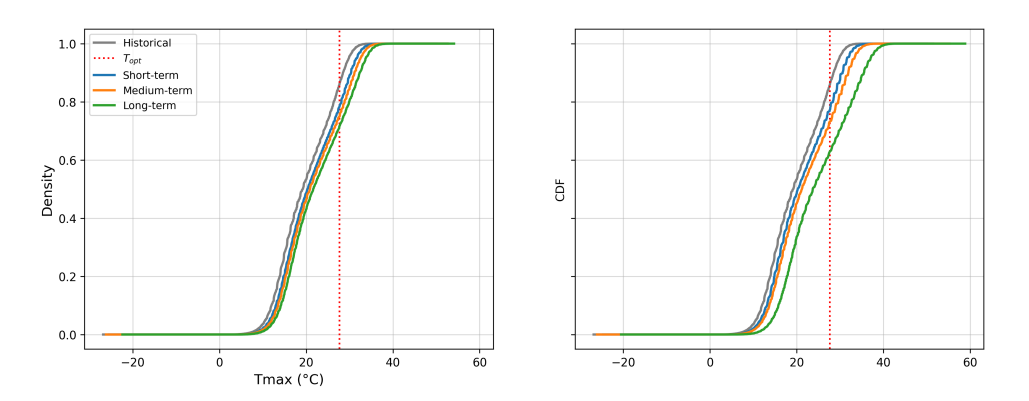


Figure 3.8: CDFs of daily maximum temperature for Barcelona: on the left SSP2-4.5, on the right SSP5-8.5.

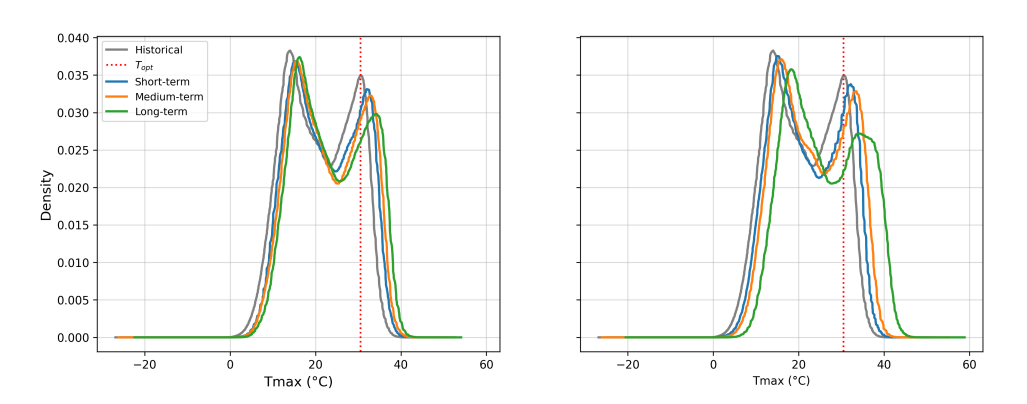


Figure 3.9: PDFs of daily maximum temperature for Athens: on the left SSP2-4.5, on the right SSP5-8.5.

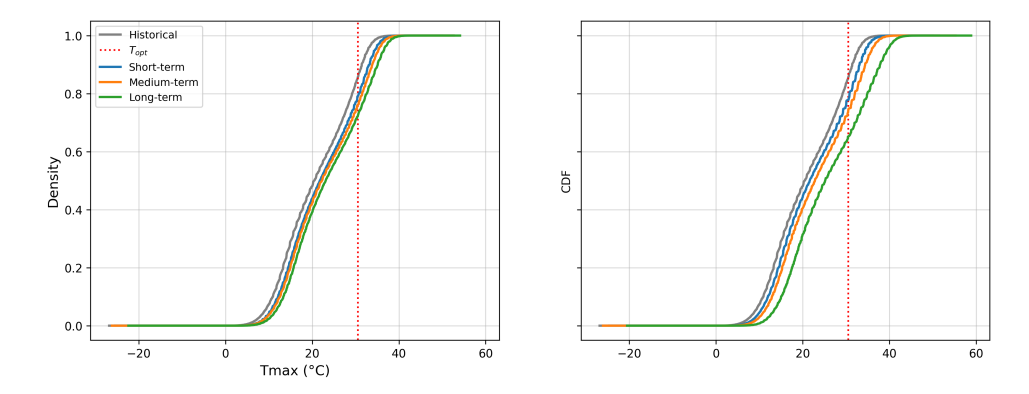


Figure 3.10: CDFs of daily maximum temperature for Athens: on the left SSP2-4.5, on the right SSP5-8.5.

Northern and central European cities such as Turin, Madrid, Belgrade and Rome also exhibit the Urban Heat Island effect. However, they are located inland, and are less influenced by the sea.

The PDFs show similar trends for Turin (Figure 3.11), Madrid (Figure 3.13) and Rome (Figure 3.17), while Belgrad (Figure 3.15) displays a comparable warming pattern under the SSP5-8.5 scenario, particularly for the long-term horizon. Belgrade is the city that shows the most evident changes in the PDFs, compared to the historical distribution (Figure 3.15), with a marked shift to temperatures above the T_{opt} . The shapes and slopes of the CDFs are similar for these cities. Considering inland urban areas, CDFs reach similar values of probability of exceeding the threshold, with differences related to the distance from the historical line.

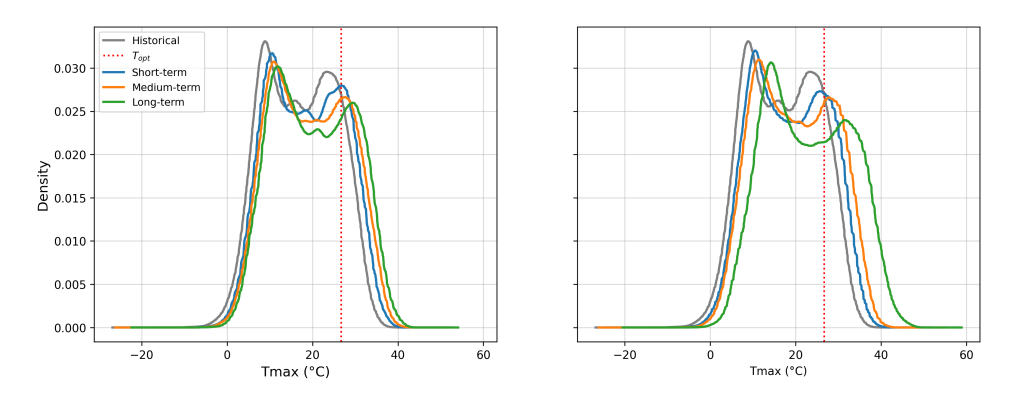


Figure 3.11: PDF of daily maximum temperature for Turin: on the left SSP2-4.5, on the right SSP5-8.5.

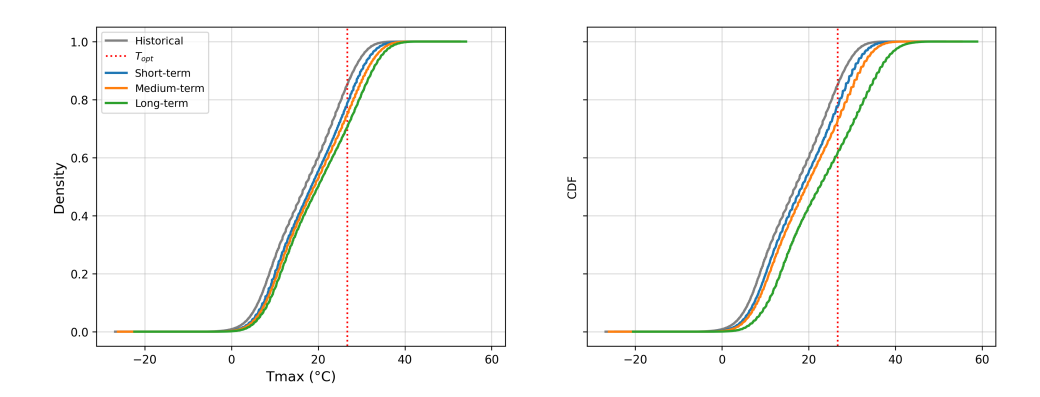


Figure 3.12: CDF of daily maximum temperature for Turin: on the left SSP2-4.5, on the right SSP5-8.5.

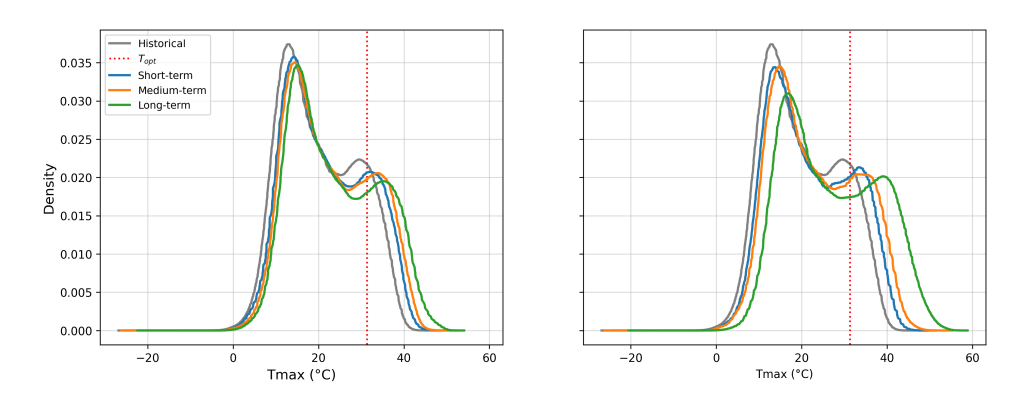


Figure 3.13: PDF of daily maximum temperature for Madrid: on the left SSP2-4.5, on the right SSP5-8.5.

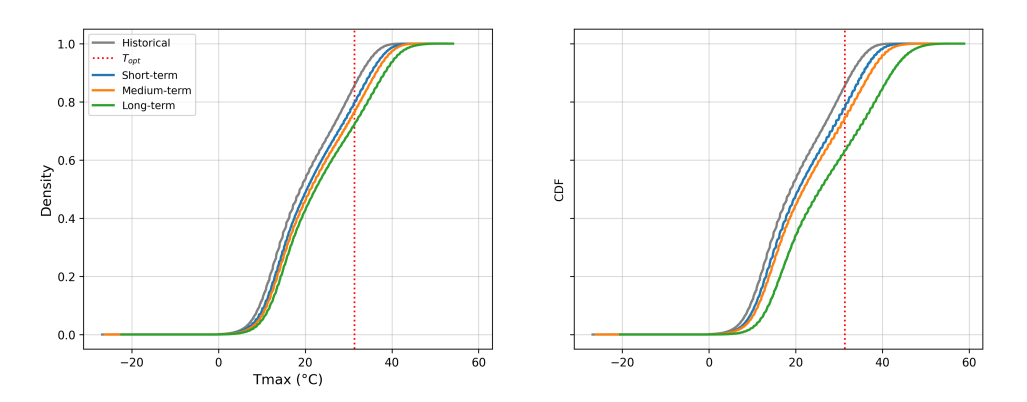


Figure 3.14: CDF of daily maximum temperature for Madrid: on the left SSP2-4.5, on the right SSP5-8.5.

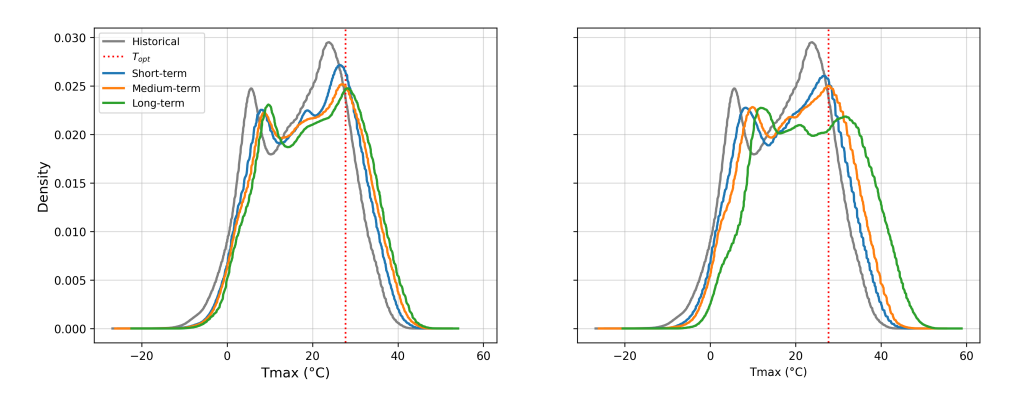


Figure 3.15: PDF of daily maximum temperature for Belgrade: on the left SSP2-4.5, on the right SSP5-8.5.

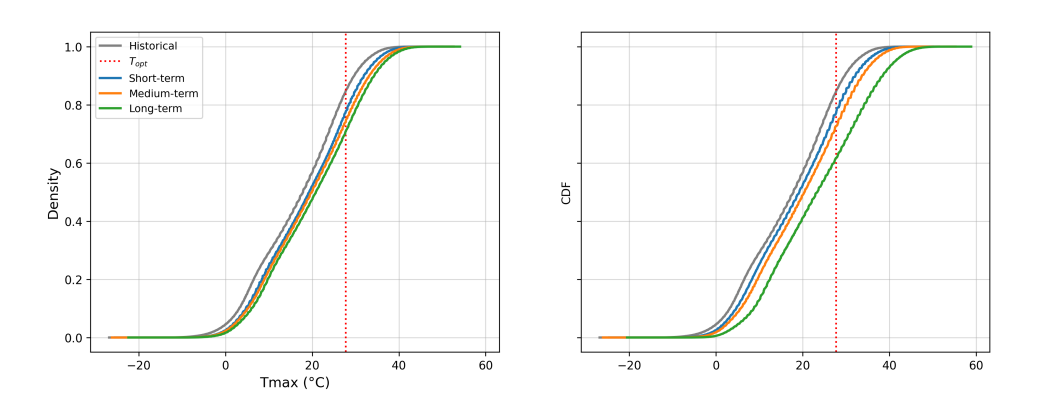


Figure 3.16: CDF of daily maximum temperature for Belgrade: on the left SSP2-4.5, on the right SSP5-8.5.

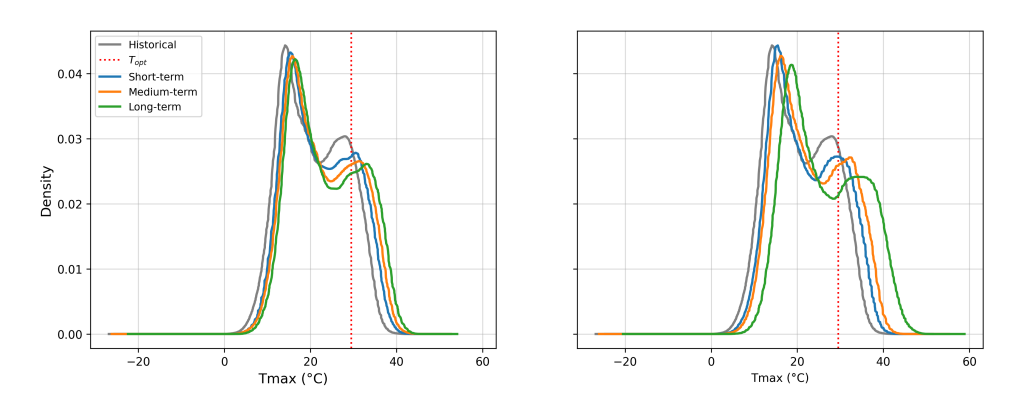


Figure 3.17: PDF of daily maximum temperature for Rome: on the left SSP2-4.5, on the right SSP5-8.5.

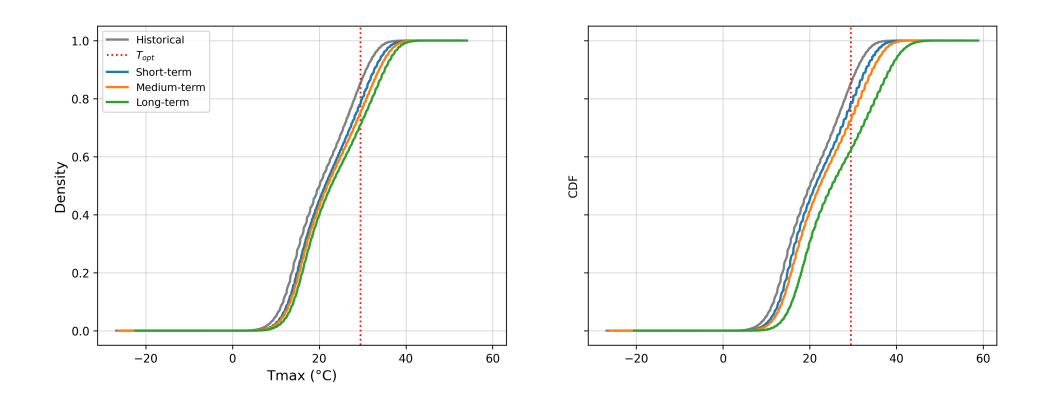


Figure 3.18: CDF of daily maximum temperature for Rome: on the left SSP2-4.5, on the right SSP5-8.5.

3.2 Excess mortality and Population Exposure

The assessment of risk for the Mediterranean population due to heat was extended to quantify potential impacts on human health, expressed in terms of excess mortality, as a percentage and relative to baseline mortality.

A multi-model approach, consistent with the one used for T_{opt} , was applied to estimate excess mortality across selected scenarios and time horizons.

Figures 3.19 and 3.20 illustrate the spatial distribution of mean excess mortality and its associated uncertainty, quantified through the Coefficient of Variation.

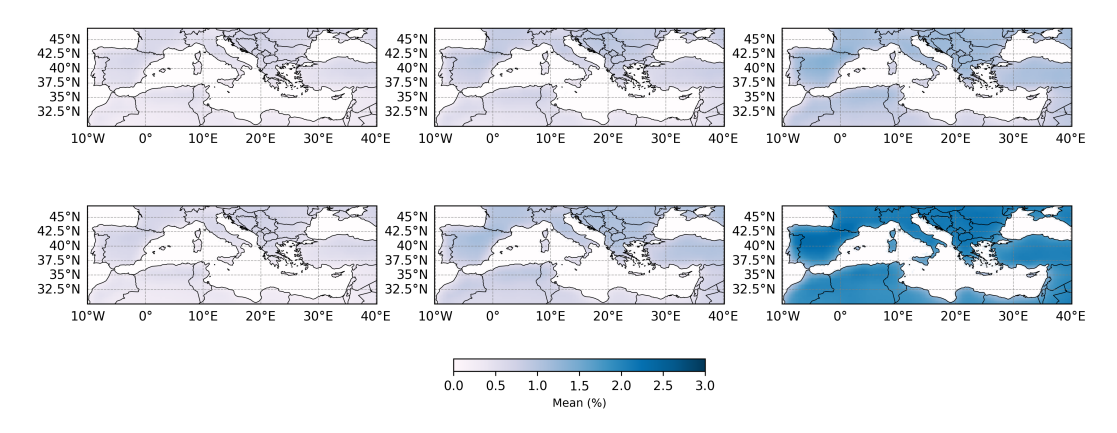


Figure 3.19: Mean of excess mortality (%) for the two scenarios (SSP2-4.5 in the first row, SSP5-8.5 in the second row) and the three time horizons: short (first column), medium (second column) and long term (third column).

Figure 3.19 indicates a generally homogeneous increase in mean excess mortality, reaching approximately 1.0-1.5% for the long term horizon under the SSP2-4.5 scenario, and up to 3% under SSP5-8.5. Although the graphs indicate a clear increasing trend, regional differences are not strongly pronounced, with excess mortality remaining relatively stable across other time horizons and for SS2-4.5, with significant increase evident for the long term SSP5-8.5 scenario.

Figure 3.20 shows the Coefficient of Variation of excess mortality across models, serving as a measure of uncertainty.

The greatest uncertainty occurs along coastlines, reflecting the increased sensitivity of these regions to local climate variability and model differences. The SSP5-8.5 scenario exhibits higher uncertainty, particularly for the long-term horizon.

Coastal variability may be also influenced by local scale processes, including wind, storms, and wave activity, which are subject to significant multi-model uncertainty.

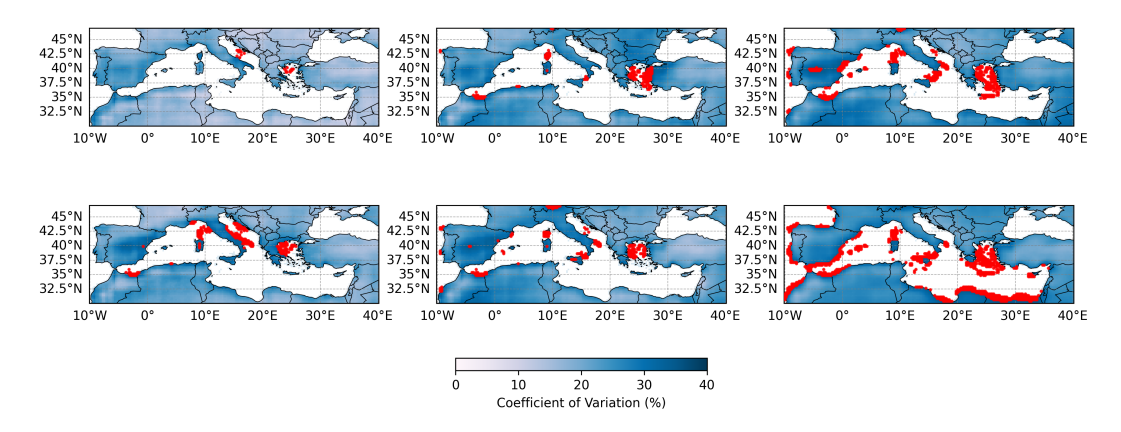


Figure 3.20: CV of excess mortality (%) for the two scenarios (SSP2-4.5 in the first row, SSP5-8.5 in the second row) and the three time horizons: short (first column), medium (second column) and long term (third column) with red marker indicating zones of higher uncertainties.

The focus of the analysis was the assessment of potential impacts related to heat on the Mediterranean population. To this end, excess mortality data were combined with population data, to identify areas at higher risk. Population density (expressed as base 10 logarithm) at each grid point was compared to excess mortality. Results presented in Appendix A, suggest no clear or significant trends between these two variables.

Scatter plots for selected urban areas (Figure 3.21) provide an examination of the relationship between historical climate conditions (T_{opt} on the x-axis), population size (represented by marker size) and future excess mortality.

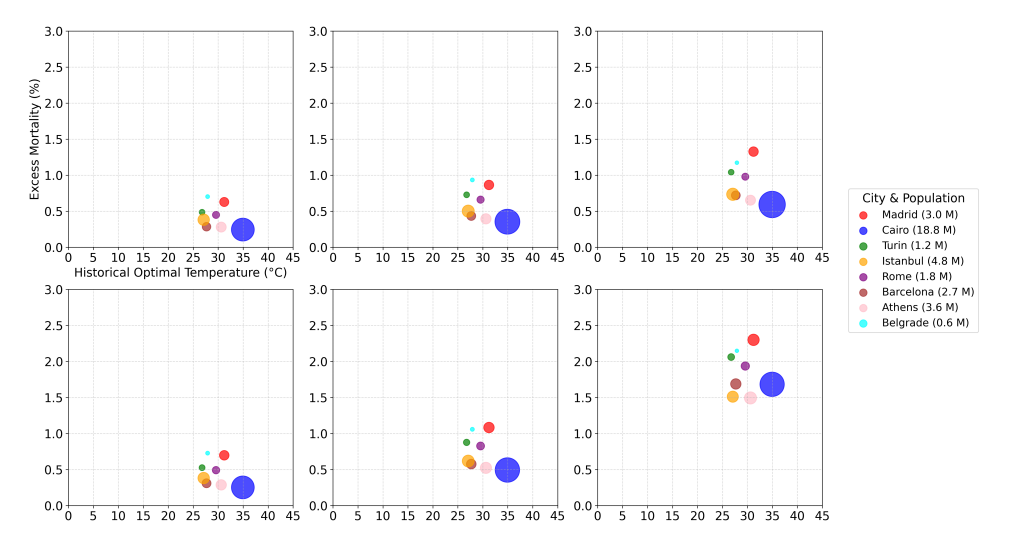


Figure 3.21: Population of considered cities as a function of T_{opt} and mean excess mortality (%) for the two scenarios (SSP2-4.5 in the first row, SSP5-8.5 in the second row) and the three time horizons: short (first column), medium (second column) and long term (third column). Marker size proportional to city population.

Southern cities, such as Cairo, exhibits higher T_{opt} value, ranging from approximately 25°C to a maximum of about 35°C (Cairo), as highlighted previously (Figure 3.1). However, the projected excess mortality remains moderate for SSP2-4.5 scenario.

In contrast, European cities, such as Madrid, Rome, Turin, and Belgrade, with lower optimum temperature value exhibit higher excess mortality, particularly under SSP5-8.5 scenario in the long-term horizon.

In general, under SSP5-8.5, a marked increase in excess mortality is projected for all cities, with Madrid showing the highest values (about 2.4%) in the long term. Overall, excess mortality values across all cities ranges between 1.5%-2.5% under the long term SSP5-8.5 scenario, consistent with spatial pattern shown previously.

The synthetic Z-score maps combine excess mortality with population density, providing a spatial representation of areas at risk. In the short-term, positive values of the index are concentrated mostly in densely populated urban areas, with negative values particularly visible in the internal zones of North Africa and in Greek islands.

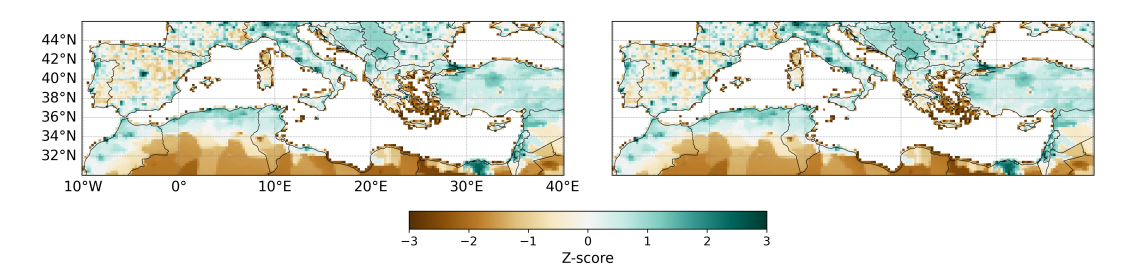


Figure 3.22: Z-score to combine excess mortality with population density for short-term and two scenarios: SSP2-4.5 on the left and SSP5-8.5 on the right.

In the medium term, areas with positive values expand slightly, with the most visible change in North Africa, with values near zero in the internal part of the continent.

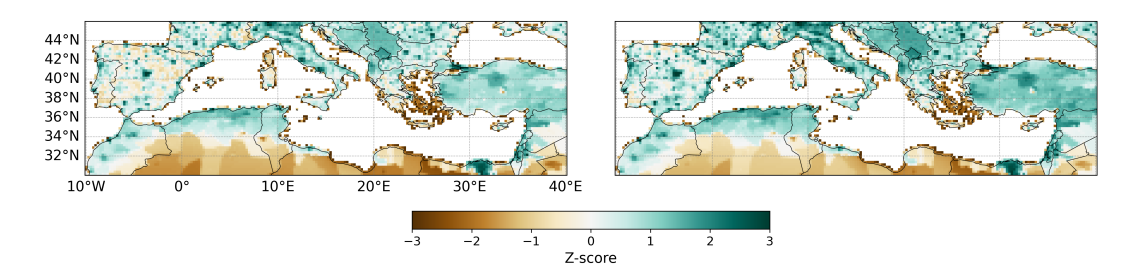


Figure 3.23: Z-score to combine excess mortality with population density for mediumterm and two scenarios: SSP2-4.5 on the left and SSP5-8.5 on the right.

In the long-term, especially under SSP5-8.5 scenario, all cells show positive values, with only a few negative zones remaining. This highlights a widespread increase in risk.

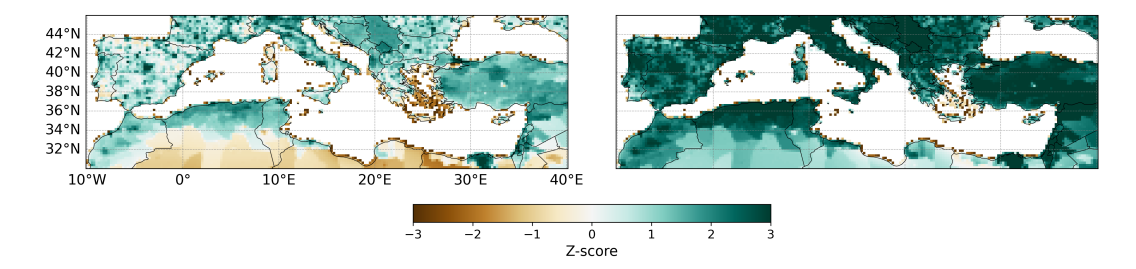


Figure 3.24: Z-score to combine excess mortality with population density for long-term and two scenarios: SSP2-4.5 on the left and SSP5-8.5 on the right.

These results highlight areas at higher risk, corresponding to urban centers where projected excess mortality intersects with high population exposure. They reflect future projections, showing the impacts of temperature extreme events on densely populated urban centers and coastal rgeions [14].

The comparison between SSP2-4.5 and SSP5-8.5 scenarios underlines the critical role of mitigation pathways, demonstrating that under the lower emission trajectories, projected risks are substantially reduced.

It is important to note that areas with higher uncertainty (with high CV values, Figure 3.20) correspond to zones with lower Z-scores, particularly along North African coastlines and some Greek islands.

Chapter 4

Discussions and Conclusions

Climate change represents one of the most crucial challenges for the future of the Mediterranean Basin, due to both its pace and magnitude. The region is particularly vulnerable to the impacts of a warming climate, most evident in the form of prolonged and more intense extreme heat events [14].

All Mediterranean countries are affected by climate change impacts [14], with significant implications for human health [18].

The region has been identified as a climate change hotspot, with projected warming rates approximately 20% above the global mean, reaching 50% in the summer period [18]. This is combined with high population exposure and vulnerability [11].

Accelerated warming trends translate into a wide range of interconnected risks for the Mediterranean Basin. Prolonged and stronger extreme heat events increase also drought and coastal flooding; uncertainties in the timing, duration, intensity, and interval between extreme climatic events put some sectors at particular risk in the region [14].

Southeastern Mediterranean countries are particularly vulnerable to coastal risk, but the exposure may become high also in the northern part of the region [14].

In terms of people, North African countries are the most exposed to sea level rise, and among these, Egypt is particularly exposed with several coastal cities at risk of inundation [14].

Overall, sea level rise is projected to increase the risk of coastal flooding, and this is amplified by climate change, particularly in river deltas [14].

Also inland areas are at risk: increasing heat waves, combined with drought and land use change, increase the likelihood of large and severe fires [14]. In addition, desertification occurs in large parts of the region, generally due to unsustainable land use. Increasing drought is projected to exacerbate desertification in North Africa and, under high warming, also in southern Spain [14]. Irrigation needs could increase by 25% in northern and two-fold in southeastern Mediterranean, with arid and southern areas at risk of insufficient water resources by 2100 [14]. Seawater intrusion is projected to cause additional risks in coastal aquifers, with severe impacts on agricultural productivity [14].

Within this complex spectrum of interconnected climate risks, this thesis focuses

specifically on the impacts of increasing heat on human health. Direct effects of extreme heat events on morbidity and mortality for population constitute one of the most urgent threats, already observable in current climate conditions, and projected to intensify in the coming decades.

By adopting the IPCC risk framework, this study translates the concepts of hazard, exposure, and vulnerability into an operational assessment. The risk caused by increasing heat is quantified in terms of excess mortality under different climate scenarios (SSP2-4.5 and SSP5-8.5) and time horizons (short, medium, and long term).

The results confirm the documented increase in health risks due to extreme heat events in the Mediterranean [14]. Results show projected increases in the excess mortality, under both emission scenarios, with the strongest effects visible under SSP5-8.5 in the long term horizon. This poses evidence on the need for adaptation measures.

The focus on the Mediterranean cities provides additional insights, highlighting slightly different projections across selected urban centers. Madrid emerges as particularly at risk, with excess mortality reaching about 2.5% under SSP5-8.5 scenario in the long-term. Other European cities, such as Rome, Turin, and Belgrade, also show significant increases in excess mortality. Southern Mediterranean cities, including Cairo and Athens, exhibit high baseline temperature but comparatively lower projected excess mortality, maybe due to differences in population acclimatization and vulnerability.

The spatial analysis of risk demonstrates that densely populated urban centers act as hotspots of heat impacts. The use of a synthetic Z-score, integrating excess mortality with population density allows for a clear identification of the most exposed areas. Also in this case, SSP5-8.5 scenario under long-term horizon shows a diffused increase in the risk, with reduced regional differences.

Excess mortality maps are smoothed and do not allow the identification of detailed regional differences. This limitation arises because excess mortality is determined as a combination of hazard (future temperature distribution), and population vulnerability (Relative Risk function), and then aggregated as multi-model mean.

Despite this, regional differences can be observed in the scatter plot for selected cities and in maps showing the synthetic index results.

Uncertainty analysis, based on the Coefficient of Variation (CV) across models, identifies regions where projections are less robust, particularly along coastlines and islands. This is especially relevant considering that approximately one-third of the Mediterranean population is concentrated along its coastal regions [18]. In fact, about 250 million people reside in coastal hydrological basins, with 120 million inhabitants concentrated in coastal regions in the southern part of Mediterranean [18].

Results can be used to identify regions at higher risks to increasing temperatures, considering that extreme heat events affect urban centers and coastal regions, causing health risks for vulnerable groups [14].

The analysis did not consider population percentage of more vulnerable groups, providing a generalized assessment of excess mortality, with respect to baseline data.

Adapting to increasing temperature impacts involves local urban health adaptation plans, which need to be integrative and assess infrastructures, urban areas, and the implementation of early warning systems [14].

In conclusion, this semi-quantitative risk assessment highlights that increasing heat will pose severe threats to human health in the Mediterranean Basin, confirming its status as one of the most exposed climate hotspot worldwide.

References

- [1] Sharon Campbell, Tomas A Remenyi, Christopher J White, and Fay H Johnston. "Heatwave and health impact research: A global review". In: *Health & place* 53 (2018), pp. 210–218 (cit. on p. 1).
- [2] IPCC. "Sections". In: Climate Change 2023: Synthesis Report. Contribution of Working Groups I, II and III to the Sixth Assessment Report of the Intergovernmental Panel on Climate Change. Ed. by Core Writing Team, H. Lee, and J. Romero. Geneva, Switzerland: IPCC, 2023, pp. 35–115. DOI: 10.59327/IPCC/AR6-9789291691647 (cit. on p. 1).
- [3] James Hansen, Makiko Sato, Reto Ruedy, Ken Lo, David W Lea, and Martin Medina-Elizade. "Global temperature change". In: *Proceedings of the National Academy of Sciences* 103.39 (2006), pp. 14288–14293 (cit. on p. 1).
- [4] Valérie Masson-Delmotte et al. "Global warming of 1.5 C". In: An IPCC Special Report on the impacts of global warming of 1.5 (2018), pp. 43–50 (cit. on p. 1).
- [5] D. Chen et al. "Framing, Context, and Methods". In: Climate Change 2021: The Physical Science Basis. Contribution of Working Group I to the Sixth Assessment Report of the Intergovernmental Panel on Climate Change. Ed. by V. Masson-Delmotte et al. Cambridge, United Kingdom and New York, NY, USA: Cambridge University Press, 2021, pp. 147–286. DOI: 10.1017/9781009157896.003 (cit. on pp. 1, 13).
- [6] Tugba Ozturk, Zeynep Pelin Ceber, Murat Türkeş, and M Levent Kurnaz. "Projections of climate change in the Mediterranean Basin by using downscaled global climate model outputs." In: *International Journal of Climatology* 35.14 (2015) (cit. on p. 2).
- [7] IPCC. Managing the Risks of Extreme Events and Disasters to Advance Climate Change Adaptation. A Special Report of Working Groups I and II of the Intergovernmental Panel on Climate Change. Ed. by C.B. Field et al. Cambridge, UK and New York, NY, USA: Cambridge University Press, 2012, p. 582 (cit. on pp. 2, 4).
- [8] A. Reisinger et al. "Annex I: Glossary". In: Climate Change 2023: Synthesis Report. Contribution of Working Groups I, II and III to the Sixth Assessment Report of the Intergovernmental Panel on Climate Change. Ed. by H. Lee Core Writing Team and J. Romero. Geneva, Switzerland: IPCC, 2023, pp. 119–130.

- DOI: 10.59327/IPCC/AR6-9789291691647.002. URL: https://www.ipcc.ch/report/ar6/syr/(cit. on pp. 2, 4, 8, 12).
- K. Poljanšek, M. Marin Ferrer, T. De Groeve, and I. Clark, eds. Science for Disaster Risk Management 2017: Knowing Better and Losing Less. EUR 28034
 EN. JRC102482. Luxembourg: Publications Office of the European Union, 2017.
 ISBN: 978-92-79-60679-3. DOI: 10.2788/842809 (cit. on p. 3).
- [10] Jeremy J Hess, Nicole A Errett, Glenn McGregor, Tania Busch Isaksen, Zachary S Wettstein, Stefan K Wheat, and Kristie L Ebi. "Public health preparedness for extreme heat events". In: *Annual Review of Public Health* 44.1 (2023), pp. 301–321 (cit. on p. 4).
- [11] Omid Mazdiyasni, Mojtaba Sadegh, Felicia Chiang, and Amir AghaKouchak. "Heat wave intensity duration frequency curve: A multivariate approach for hazard and attribution analysis". In: *Scientific reports* 9.1 (2019), p. 14117 (cit. on pp. 4, 35).
- [12] Y Luo, X Cheng, B-J He, and BJ Dewancker. "Identification and assessment of heat disaster risk: a comprehensive framework based on hazard, exposure, adaptation and vulnerability". In: *International Journal of Environmental Science and Technology* 22.12 (2025), pp. 11275–11294 (cit. on pp. 4, 5).
- [13] S.I. Seneviratne et al. "Weather and Climate Extreme Events in a Changing Climate". In: Climate Change 2021: The Physical Science Basis. Contribution of Working Group I to the Sixth Assessment Report of the Intergovernmental Panel on Climate Change. Ed. by V. Masson-Delmotte et al. Cambridge University Press, 2021, pp. 1513–1766. DOI: 10.1017/9781009157896.013 (cit. on p. 4).
- [14] E. Ali, W. Cramer, J. Carnicer, E. Georgopoulou, N.J.M. Hilmi, G. Le Cozannet, and P. Lionello. "Cross-Chapter Paper 4: Mediterranean Region". In: Climate Change 2022: Impacts, Adaptation and Vulnerability. Contribution of Working Group II to the Sixth Assessment Report of the Intergovernmental Panel on Climate Change. Ed. by H.-O. Pörtner et al. Cambridge, UK and New York, NY, USA: Cambridge University Press, 2022, pp. 2233–2272. DOI: 10.1017/9781009325844.021 (cit. on pp. 5–8, 34–37).
- [15] Filippo Giorgi and Piero Lionello. "Climate change projections for the Mediterranean region". In: *Global and planetary change* 63.2-3 (2008), pp. 90–104 (cit. on p. 5).
- [16] European Environment Agency and UNEP/MAP. Horizon 2020 Mediterranean report: Toward shared environmental information systems. Luxembourg: Publications Office of the European Union, 2014. ISBN: 978-92-9213-430-3. DOI: 10.2800/13326. URL: https://planbleu.org/wp-content/uploads/2014/05/h2020_mediterranean_report2014.pdf (cit. on pp. 6, 17).

- [17] Cristina Linares, Julio Díaz, Maya Negev, Gerardo Sánchez Martínez, Roberto Debono, and Shlomit Paz. "Impacts of climate change on the public health of the Mediterranean Basin population-current situation, projections, preparedness and adaptation". In: *Environmental research* 182 (2020), p. 109107 (cit. on p. 7).
- [18] Wolfgang Cramer, Joël Guiot, and Katarzyna Marini, eds. Climate and Environmental Change in the Mediterranean Basin Current Situation and Risks for the Future. First Mediterranean Assessment Report. Marseille, France: Union for the Mediterranean, Plan Bleu, UNEP/MAP, 2020, p. 632. ISBN: 978-2-9577416-0-1. DOI: 10.5281/zenodo.7224821. URL: https://www.medecc.org/first-mediterranean-assessment-report-mar1/ (cit. on pp. 7-9, 17, 35, 36).
- [19] World Climate Research Programme (WCRP). CMIP Overview Coupled Model Intercomparison Project. https://wcrp-cmip.org/cmip-overview/ (cit. on p. 10).
- [20] Climate.gov. Climate Models Climate Data Primer. https://www.climate.gov/maps-data/climate-data-primer/predicting-climate/climate-models (cit. on pp. 10, 11).
- [21] Geophysical Fluid Dynamics Laboratory. *Earth System Models*. 2025. URL: https://www.gfdl.noaa.gov/earth-system-models/(cit. on p. 11).
- [22] Veronika Eyring, Sandrine Bony, Gerald A Meehl, Catherine A Senior, Bjorn Stevens, Ronald J Stouffer, and Karl E Taylor. "Overview of the Coupled Model Intercomparison Project Phase 6 (CMIP6) experimental design and organization". In: Geoscientific Model Development 9.5 (2016), pp. 1937–1958 (cit. on pp. 11, 12).
- [23] Brian C O'Neill et al. "The scenario model intercomparison project (ScenarioMIP) for CMIP6". In: *Geoscientific Model Development* 9.9 (2016), pp. 3461–3482 (cit. on p. 12).
- [24] Bridget Thrasher, Weile Wang, Andrew Michaelis, Forrest Melton, Tsengdar Lee, and Ramakrishna Nemani. "NASA global daily downscaled projections, CMIP6". In: *Scientific data* 9.1 (2022), p. 262 (cit. on p. 14).
- [25] Andrew W Wood, Lai R Leung, Venkataramana Sridhar, and Dennis P Lettenmaier. "Hydrologic implications of dynamical and statistical approaches to downscaling climate model outputs". In: *Climatic change* 62.1 (2004), pp. 189–216 (cit. on p. 14).
- [26] NASA Center for Climate Simulation (NCCS). NEX-GDDP-CMIP6. https://www.nccs.nasa.gov/services/data-collections/land-based-products/nex-gddp-cmip6 (cit. on p. 14).
- [27] Yasushi Honda et al. "Heat-related mortality risk model for climate change impact projection". In: *Environmental health and preventive medicine* 19.1 (2014), pp. 56–63 (cit. on pp. 14, 18–20, 22).

- [28] World Bank Group. Climate Change Knowledge Portal. 2025. URL: https://climateknowledgeportal.worldbank.org/(cit. on p. 15).
- [29] Marta Ellena, Joan Ballester, Paola Mercogliano, Elisa Ferracin, Giuliana Barbato, Giuseppe Costa, and Vijendra Ingole. "Social inequalities in heat-attributable mortality in the city of Turin, northwest of Italy: a time series analysis from 1982 to 2018". In: *Environmental Health* 19.1 (2020), p. 116 (cit. on p. 16).
- [30] Annalisa Di Bernardino, Serena Falasca, Anna Maria Iannarelli, Stefano Casadio, and Anna Maria Siani. "Effect of heatwaves on urban sea breeze, heat island intensity, and outdoor thermo-hygrometric comfort in Rome (Italy)". In: *Urban Climate* 52 (2023), p. 101735 (cit. on p. 16).
- [31] Domingo Rasilla, Fernando Allende, Alberto Martilli, and Felipe Fernández. "Heat waves and human well-being in Madrid (Spain)". In: *Atmosphere* 10.5 (2019), p. 288 (cit. on p. 16).
- [32] Carina Serra, Xavier Lana, Maria-Dolors Martínez, Blanca Arellano, Josep Roca, and Rolando Biere. "Summer heatwaves trends and hotspots in the Barcelona Metropolitan Region (1914–2020)". In: *Theoretical and Applied Climatology* 155.6 (2024), pp. 4681–4702 (cit. on pp. 16, 25).
- [33] Merve Yılmaz, Yiğitalp Kara, Hazal Cansu Çulpan, Günay Can, and Hüseyin Toros. "Detection and regional analysis of heatwave characteristics in İstanbul". In: Sustainable Cities and Society 97 (2023), p. 104789 (cit. on p. 16).
- [34] Amira N Mostafa, Stéphane C Alfaro, Sayed M Robaa, Ashraf S Zakey, and Mohamed M Abdel Wahab. "Heatwaves and Their Impact on Air Quality in Greater Cairo, Egypt". In: *Atmosphere* 15.6 (2024), p. 637 (cit. on p. 16).
- [35] George Katavoutas and Dimitra Founda. "Response of urban heat stress to heat waves in Athens (1960–2017)". In: *Atmosphere* 10.9 (2019), p. 483 (cit. on pp. 16, 25).
- [36] Miroslava Unkašević and Ivana Tošić. "An analysis of heat waves in Serbia". In: Global and planetary change 65.1-2 (2009), pp. 17–26 (cit. on p. 17).
- [37] Antonio Gasparrini et al. "Mortality risk attributable to high and low ambient temperature: a multicountry observational study". In: *The lancet* 386.9991 (2015), pp. 369–375 (cit. on p. 18).
- [38] Linda Krummenauer, Boris F Prahl, Luís Costa, Anne Holsten, Carsten Walther, and Jürgen P Kropp. "Global drivers of minimum mortality temperatures in cities". In: *Science of the total environment* 695 (2019), p. 133560 (cit. on pp. 18, 23).
- [39] Adelin Albert and Lixin Zhang. "A novel definition of the multivariate coefficient of variation". In: *Biometrical Journal* 52.5 (2010), pp. 667–675 (cit. on p. 19).
- [40] Alexander E Curtis, Tanya A Smith, Bulat A Ziganshin, and John A Elefteriades. "The mystery of the Z-score". In: *Aorta* 4.04 (2016), pp. 124–130 (cit. on p. 20).

- [41] Junzhe Bao, Xudong Li, and Chuanhua Yu. "The construction and validation of the heat vulnerability index, a review". In: *International journal of environmental research and public health* 12.7 (2015), pp. 7220–7234 (cit. on pp. 20, 21).
- [42] Stephen J Vavrus, Michael Notaro, and David J Lorenz. "Interpreting climate model projections of extreme weather events". In: Weather and Climate Extremes 10 (2015), pp. 10–28 (cit. on p. 23).
- [43] George Zittis et al. "Business-as-usual will lead to super and ultra-extreme heat-waves in the Middle East and North Africa". In: *Npj Climate and Atmospheric Science* 4.1 (2021), p. 20 (cit. on p. 24).

Appendix A

Appendix A

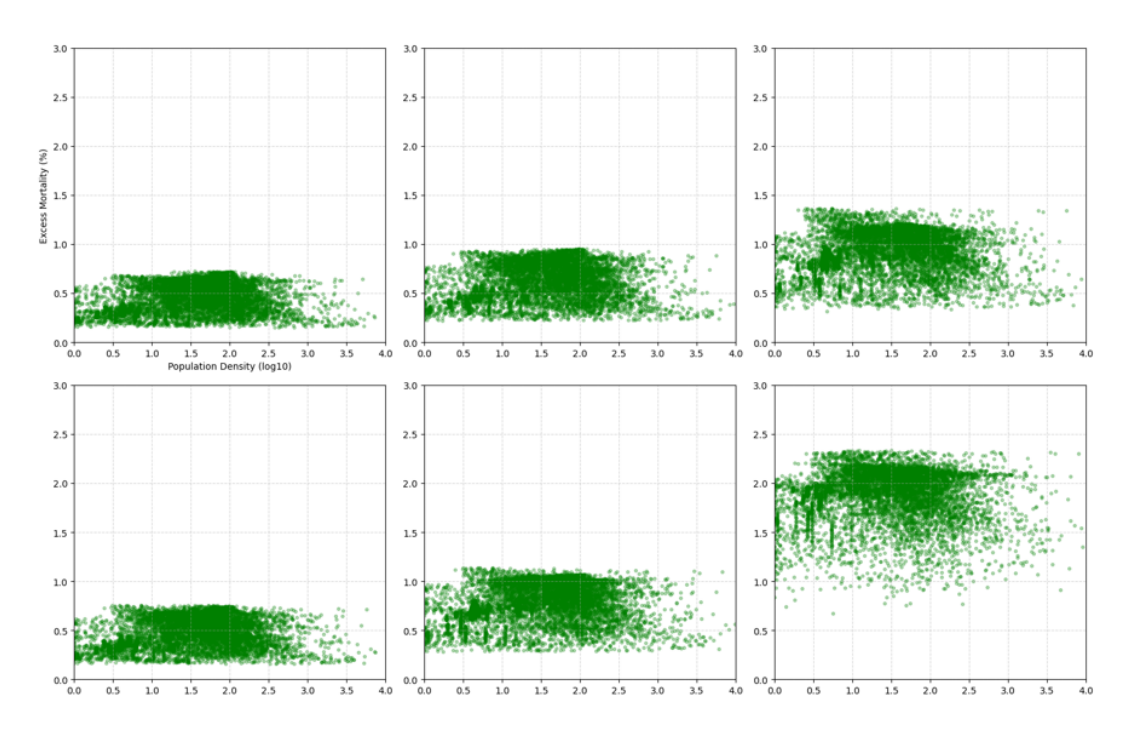


Figure A.1: Population density (log10) related to excess mortality mean (%): SSP2-4.5 in the first row, SSP5-8.5 in the second row and the three time horizons: short (first column), medium (second column) and long term (third column).